IGNITION MODELING AND THE CRITICAL DECAY RATE CONCEPT

J. E. SHEPHERD
GRADUATE AEROSPACE LABORATORIES
CALIFORNIA INSTITUTE OF TECHNOLOGY
PASADENA, CA 91125

GALCIT REPORT EDL2019.002

Published by California Institute of Technology

IGNITION MODELING AND THE CRITICAL DECAY RATE CONCEPT

Joseph E. Shepherd
Graduate Aerospace Laboratories
California Institute of Technology
Pasadena CA 91125

GALCIT REPORT EDL2019-002

February 9, 2020 - Revised December 9, 2020

Abstract

Models of ignition are considered for transient compression followed by expansion of a reactive gas volume. Under such conditions, the critical conditions for ignition depend on the competition between chemical reaction and work done due to imposed volume or pressure changes. This competition can be characterized by a critical decay rate that defines the boundary between ignition and non-ignition. Zero-dimensional unsteady models are formulated for transient processes and numerical solutions are used to obtain critical conditions for H_2-O_2-steam mixtures at both laboratory and typical nuclear power reactor initial conditions for a range of volume compression ratios between 5 and 50. An analytical model for critical decay rate is formulated and solved for the case of sudden compression followed by exponential increase in volume. Explicit expressions for critical value of the decay time constant are compared with numerical solutions with a detailed chemical reaction mechanism and realistic thermochemistry. Critical pulse widths are computed for the ignition of an explosion by a Gaussian volume history of inverse volume which models compression followed by expansion. Validation of the chemical reaction model is performed and an evaluation is carried out of the reaction pathways under low-temperature (900-1050 K) and high-pressure (10-20 MPa) conditions present at maximum compression.

Contents

List of Figures

List of Tables

1 Introduction

Idealized models of adiabatic compression ignition of a time-varying gas volume are developed and used to examine the explosion of hydrogen-oxygen mixtures for a range of initial conditions. These idealized models treat several situations associated with adiabatic explosions such as shock waves, rapid compression machines, and water hammer induced volume change. All of these models have in common the idealization of a homogeneous ideal gas mixture with spatially-uniform thermodynamic conditions that depend only on time. The gas mixture consists of a set of species which react through a network of reactions with a realistic models of individual reaction rates and thermodynamic properties for each species. Numerical solutions are given for four situations: a) rapid (instantaneous) isentropic compression followed by constant-volume conditions; b) instantaneous isentropic compression followed by expansion at an exponential rate; c) simulation of a rapid compression machine, a finite-duration isentropic compression followed by slow expansion; d) a compression pulse with a finite duration isentropic compression immediately followed by an isentropic expansion, the inverse volume is modeled as having a Gaussian variation with time.

Special consideration is given to the critical conditions for ignition when the isentropic compression is followed immediately by expansion. In the case of rapid compression followed by expansion, there is a critical rate of expansion that separates the explosive vs. non-explosive solutions. For an exponential dependence of volume on time, the process is characterized by a time constant which specifies the rate of volume change which in turn determines the rate of temperature and pressure decay. The critical value of the time constant can be computed numerically using detailed chemical reaction mechanisms and estimated analytically by using asymptotic analysis of a model one-step irreversible reaction. The critical value of the time constant is approximately an order of magnitude larger than the adiabatic constant volume explosion time. Comparisons of the numerical simulations with the analytical results shows reasonable agreement for sufficiently large values of the effective activation energy. For the Gaussian pulse of volume compression, there is a critical pulse width that separates explosive from non-explosive outcomes. The pulse width must be larger than the critical value in order for an explosion to occur.

The critical decay time for exponential expansion model as well as the critical pulse width for the Gaussian pulse model are computed for hydrogen-oxygen-steam mixtures for isentropic compression starting from initial conditions characteristics of laboratory experiments (Coronel et al., 2020) as well as nuclear power plant primary coolant systems. Examination of reaction pathways for temperatures between 900 and 1200 K and pressures between 4 and 21 MPa reveals that the critical conditions for ignition for result in critical reaction pathways being dominated by H_2O_2 and HO_2 during the induction period leading up to the onset of the chain-branching reactions. This result is specific to these mixtures and conditions.

2 Modeling

Ignition in an adiabatic compression event can be modeled using the first law of thermodynamics

$$\mathrm{d}e = -P\mathrm{d}v \ , \tag{1}$$

if heat transfer and dissipative processes can be neglected. For an ideal gas, the internal energy can be represented as a sum over the (mass specific) internal energies e_i of each of the k species weighted by the mass fractions Y_i

$$e = \sum_{i=1}^{k} Y_i e_i(T) \ . \tag{2}$$

Using the definition of species specific heat

$$c_{v,i} = \frac{\mathrm{d}e_i}{\mathrm{d}T} \ , \tag{3}$$

and mixture specific heat

$$c_v = \sum_{i=1}^{k} Y_i c_{v,i} \ , \tag{4}$$

the time rate of change of temperature is given by

$$\frac{\mathrm{d}T}{\mathrm{d}t} = -\frac{1}{c_v}\sum_{i=1}^{k} e_i \frac{\mathrm{d}Y_i}{\mathrm{d}t} - \frac{P}{c_v}\frac{\mathrm{d}v}{\mathrm{d}t} \ . \tag{5}$$

Introducing the ideal gas law

$$Pv = RT \ , \tag{6}$$

the energy equation can be rewritten as

$$\frac{\mathrm{d}T}{\mathrm{d}t} = -\frac{1}{c_v}\sum_{i=1}^{k} e_i \frac{\mathrm{d}Y_i}{\mathrm{d}t} - T\frac{R}{c_v}\frac{1}{v}\frac{\mathrm{d}v}{\mathrm{d}t} \ . \tag{7}$$

The rate of change of the species mass fractions can be computed using a chemical reaction mechanism and set of rate constants

$$\frac{\mathrm{d}Y_i}{\mathrm{d}t} = \frac{W_i\dot{\omega}_i}{\rho} \qquad i = 1, 2, \ldots, k \ , \tag{8}$$

where $\dot{\omega}_i$ is the net molar production rate, W_i is the molar mass of species i and $\rho = 1/v$ is the mass density. Substituting (8) into (7), the final form of the energy balance equation is

$$\frac{\mathrm{d}T}{\mathrm{d}t} = \underbrace{-\frac{1}{c_v}\sum_{i=1}^{k} e_i \frac{W_i\dot{\omega}_i}{\rho}}_{\text{chemical}} \underbrace{- T\frac{R}{c_v}\frac{1}{v}\frac{\mathrm{d}v}{\mathrm{d}t}}_{\text{work}} \ . \tag{9}$$

For exothermic reactions, the first term on the right-hand side is positive. If we consider variations in pressure rather than volume as being specified, the appropriate starting point is the enthalpy form of the first law

$$\mathrm{d}h = v\,\mathrm{d}P \ , \tag{10}$$

which gives that analogous expression

$$\frac{\mathrm{d}T}{\mathrm{d}t} = -\frac{1}{c_p}\sum_{i=1}^{k} h_i \frac{\mathrm{d}Y_i}{\mathrm{d}t} + T\frac{R}{c_p}\frac{1}{P}\frac{\mathrm{d}P}{\mathrm{d}t} \ , \tag{11}$$

in terms of the mixture specific heat at constant pressure

$$c_p = \sum_{i=1}^{k} Y_i c_{p,i} \ , \qquad c_{p,i} = \frac{\mathrm{d}h_i}{\mathrm{d}T} \ . \tag{12}$$

An explosion will occur only if the temperature increase associated with the exothermic reactions that contribute to the "chemical" term can balance and ultimately exceed any temperature decrease associated with the "work" term. If the volume $v(t)$ decreases rapidly and is held constant at a sufficiently small value, an explosion will occur and is marked by a sudden increase of temperature at the end of an induction period associated with the nearly thermal neutral processes associated with the generation of a growing pool of radical and intermediate species. This occurs in rapid compression machines with locking mechanisms (Goldsborough et al., 2017) and behind shock waves. The induction time t_i is usually[1] defined as the time elapsed from the end of compression to the onset of the rapid rise

[1]Other definitions, such as the time to an chemiluminescence emission peak or maximum rate of change of pressure or temperature, are also used to characterize ignition delays

in temperature. If the volume immediately starts to increase after the minimum is reached, there is the potential for quenching the reaction if the temperature decreases too rapidly for the energy release by the chemical reaction to compensate. That can happen in free-piston compressors and bubble collapse by pressure transients in liquids.

The temperature equations (9) and (11) are equivalent descriptions of adiabatic compression with time-dependent volume histories. The choice of which version of the temperature equation to use in modeling is a matter of convenience. Pressure histories are usually reported for shock tube experiments so modelers use some form of (11) whereas rapid compression effective volume-time data are usually reported and used in (9) for validation studies. During the non-reactive phase of a reversible compression or expansion process the volume and pressure histories are uniquely related by the isentropic constraint

$$\left(\frac{\mathrm{d}P}{\mathrm{d}v}\right)_s = -\gamma = -\frac{c_p}{c_v} \,, \tag{13}$$

which has been used by some authors (Chaos and Dryer, 2010) to convert pressure histories into volume histories required by some modeling software. More generally, the changes in P, v, and T are related by the ideal gas relation $Pv = RT$, which can be differentiated to show the exact equivalence of (9) to (11) taking into account the dependence of R on the composition $\mathbf{Y} = (Y_1, Y_2, \ldots, Y_k)$.

Accounting for the heat transfer and other nonideal features that result in pressure changes after rapid compression is particularly important when using the results of experiments to infer reaction rates and validate reaction mechanisms. For rapid compression machines it is particularly important to consider heat transfer (Goldsborough et al., 2012) whereas for shock tubes it important to account for the time dependence of the pressure (Chaos and Dryer, 2010, Li et al., 2008) created by gas dynamic effects (Grogan et al., 2015, Grogan and Ihme, 2018). Heat transfer can also be significant in shock tubes when considering low-temperature ignition with long ignition delay times. Strategies for improving the steadiness and uniformity of conditions following shock reflection have been proposed (Campbell et al., 2015a,b) for these cases. In some high-temperature situations, significant vibrational-translational nonequilibrium (Campbell et al., 2017) can occur behind shock waves and has to be accounted for in interpreting short ignition delay times. The present study is concerned with ideal processes that are adiabatic; for completeness a brief discussion is given in the next section of how these models can be extended to treat heat transfer.

Heat Transfer

Heat transfer between the gas and the surrounding container of volume V or natural convection over hot surfaces of area S can play a significant role in ignition processes. In purely thermal ignition using hot surfaces to increase the gas temperature, heat transfer is the dominant process with critical conditions resulting from a balance between chemical energy release and thermal energy transfer between the gas and surroundings. The simplest models of these processes use a control volume model and engineering representations of the thermal energy transfer rates. The energy equation for a volume V with including heat loss $\dot{q}$ per unit area is

$$\rho V \frac{\mathrm{d}e}{\mathrm{d}t} = -S\dot{q} - P\frac{\mathrm{d}V}{\mathrm{d}t} \,. \tag{14}$$

or

$$\frac{\mathrm{d}e}{\mathrm{d}t} = -\frac{S}{\rho V}\dot{q} - P\frac{1}{\rho V}\frac{\mathrm{d}V}{\mathrm{d}t} \,. \tag{15}$$

In terms of temperature, this can be written

$$\frac{\mathrm{d}T}{\mathrm{d}t} = -\frac{1}{c_v}\sum_{i=1}^{k} e_i \frac{\mathrm{d}Y_i}{\mathrm{d}t} - \frac{S}{V}\frac{\dot{q}}{\rho c_v} - T\frac{R}{c_v}\frac{1}{v}\frac{\mathrm{d}v}{\mathrm{d}t} \tag{16}$$

From this version of the energy equation it is clear that thermal energy transfer plays the same role as the work term in the variable volume models. Depending on the direction of thermal energy exchange, the heat transfer can either promote or quench the reaction processes. Transferring thermal energy from the surroundings to the gas can initiate chemical reactions and lead to ignition. However, if the direction of the thermal energy transport is reversed and energy is transported from the gas into the surroundings, this will have the effect of lengthening the ignition time and can in extreme cases, prevent an explosive reaction from occurring.

The classical model of ignition of a gas volume in a hot vessel is known as *autoignition* (Semenov, 1959) and is based on considering a constant volume and the standard engineering model for $\dot{q}$ with a heat transfer coefficient h to represent the thermal energy exchange, $\dot{q} = h(T - T_w)$ where T_w is the surface temperature. Neglecting the conjugate heat transfer (the temperature rise on the surface of an ignition vessel is usually small during the ignition transient) and taking the wall temperature T_w to be constant, the energy equation has the form

$$\frac{\mathrm{d}T}{\mathrm{d}t} = -\frac{1}{c_v}\sum_{i=1}^{k} e_i \frac{\mathrm{d}Y_i}{\mathrm{d}t} - \frac{S}{V}\frac{h}{\rho c_v}(T - T_w) \ . \tag{17}$$

The critical conditions for explosion are found by considering the possible steady solutions to this equation. Supercritical conditions result the dominance of chemical energy release over heat loss, leading to an exponential increase in temperature signifying explosion. Subcritical conditions result in the dominance of heat loss over chemical reaction and the gas temperature decreases, signifying the failure to initiate an explosion. Critical conditions have a balance between chemical energy release and heat losses, resulting in a constant value of gas temperature, also signifying the failure to initiate an explosion although the reactants will be consumed by the steady-state reaction process. This *Semenov* model of thermal explosion predicts that for an explosion to take place, the gas pressure or wall temperature must exceed critical values. These critical values are predicted (Semenov, 1959) to depend on a combination of parameters including the chemical reaction rates, heat of reaction, surface-to-volume ratio and heat transfer coefficient.

An extension of the classical model of autoignition is discussed by Boettcher et al. (2012, 2014) and Melguizo-Gavilanes et al. (2019) who consider a time-dependent wall temperature $T_w(t)$ and constant volume explosion. The energy equation for this case is

$$V\rho c_v \frac{\mathrm{d}T}{\mathrm{d}t} = -V\rho \sum_{i=1}^{k} e_i \frac{\mathrm{d}Y_i}{\mathrm{d}t} + Sh(T_w(t) - T) \ , \tag{18}$$

and the species evolve according to the kinetic mechanism

$$\frac{\mathrm{d}Y_i}{\mathrm{d}t} = \frac{W_i \dot{\omega}_i}{\rho} \qquad i = 1, 2, \ldots, k \ . \tag{19}$$

The special case of constant wall temperature was considered by Semenov who formulated the criteria for explosion in terms of the balance between energy addition and loss in the context of model one-step reaction mechanisms. Boettcher extended this treatment to a wall temperature increasing linearly with time

$$T_w = T_o + \alpha t \ . \tag{20}$$

Melguizo-Gavilanes considered the two-dimensional transient development of the explosion and the influence of non-uniform wall temperature for this situation. The conclusion of the experimental, analytical and numerical studies with increasing wall temperature is that there is a critical value of the heating rate. For sufficiently slow heating, small α, the consumption of the reactants will occur without an obvious pressure or temperature transient in the gas and for sufficiently fast heating, large α, the consumption of reactants occurs explosively with a rapid pressure and temperature transient in the gas. There is a well defined critical value α_c that separates these two cases.

3 Adiabatic Constant-Volume Explosion

For a given fuel-oxidizer composition and compression ratio[2], the ideal state at the end of an adiabatic and reversible compression can be determined by a simple thermodynamic computation assuming the compression process is non-reactive and isentropic. This is an approximate model for ignition in a rapid compression machine or compression of gas bubble in a liquid. For a non-reactive shock wave, the solution of shock jump conditions will determine the pressure and temperature immediately behind the shock wave. A common approximation is that the explosion process following compression occurs with no volume change. For this situation the explosion process is simulated by integrating (7) and (8) with $\mathrm{d}v/\mathrm{d}t = 0$.

The conditions after an ideal (reversible) adiabatic and nonreactive compression from an initial state with conditions (T_o, P_0) are found by first computing the initial entropy

$$s_0 = s(T_0, \rho_0, \mathbf{Y}_0) \tag{21}$$

where $\rho_0 = P_0/RT_0$ and then solving implicitly for the compressed gas temperature T_1 and density ρ_1 for a given compression ratio

$$CR = \rho_1/\rho_0 = v_0/v_1 \tag{22}$$

assuming an isentropic compression, $s_1 = s_0$ = constant and fixed (frozen) composition $\mathbf{Y}_1 = \mathbf{Y}_0$

$$s_0 = s(T_1, \rho_1, \mathbf{Y}_0) \tag{23}$$

then computing $P_1 = \rho_1 RT_1$. The compressed gas state is given in Table 1 for a range of compression ratios between 15 and 50 for a $H_2 + \frac{1}{2}O_2$ mixture initially at standard conditions.

The reaction process at constant volume is computed by setting $dv/dt = 0$ and numerical integration of (7) and (8) using the Cantera software package (Goodwin et al., 2017) and the routine demo_cv of the Shock and Detonation Toolbox. The thermodynamic properties and the detailed chemical kinetic model used were from Hong et al. (2011), the Cantera .cti format version is available online. The time to explosion t_i was defined at the time at which the maximum temperature time rate of change occurs relative to the instantaneous increase of temperature and pressure of the ideal compression process.

$$\left.\frac{\mathrm{d}T}{\mathrm{d}t}\right|_{t_i} = \text{maximum} \tag{24}$$

The time to explosion is determined primarily by the thermally-neutral reactions generating radicals and intermediates in the induction period that proceeds the exothermic reactions that create the rapid temperature and pressure rise associated with the explosion. These reactions have significant temperature dependence due to the energy barriers associated with the rate limiting steps for the generation of radical species. The majority of the reaction processes that transform chemical into thermal energy occurs within a time t_r which is on the order of 1-10 $\times 10^{-9}$ s (Table 1), determined by the rates of reactions which are exothermic reactions and occur rapidly if there are no energy barriers for these processes. The time t_r is arbitrarily defined by the time difference between the instant of temperature rise corresponding to 0.1 and 0.9 of the adiabatic explosion temperature rise, $\Delta T_a = T_a - T_0$.

$$t_r = t_{0.9\Delta T_a} - t_{0.1\Delta T_a} \tag{25}$$

The adiabatic, constant-volume explosion conditions are computed by solving the implicit relationship for conservation of energy between reactants and products with thermochemical equilibrium for the product species.

$$e(T_a, \mathbf{Y}^{eq}) = e(T_1, \mathbf{Y}_0) \tag{26}$$

and using the ideal gas relation to compute pressure, accounting for the product species distribution $\mathbf{Y}^{eq}$ at equilibrium to compute the gas constant R_a.

$$P_a = \rho_1 R_a T_a \tag{27}$$

[2]Compression ratio CR is defined as the ratio of initial (maximum) to final (minimum) volume.

As discussed in Bane et al. (2010), the effective activation energy and reaction order for a one-step reaction model that has the same induction time and sensitivity to initial conditions can be determined from computations of t_i for a detailed reaction mechanisms from perturbations of initial temperature and density. The effective activation energy is

$$E_a = \tilde{R} T_1 \left(-\frac{T_1}{t_i} \left(\frac{\partial t_i}{\partial T_1} \right)_\rho + 2 \right) \tag{28}$$

The derivative of induction time with respect to initial temperature is obtained by finite differences.

$$\left(\frac{\partial t_i}{\partial T_1} \right)_\rho \approx \frac{t_i(T_1 + \Delta T) - t_i(T_1)}{\Delta T} \tag{29}$$

The effective reaction order is

$$n_\rho = -\frac{\rho_1}{t_i} \left(\frac{\partial t_i}{\partial \rho_1} \right)_{T_1} + 1 \; . \tag{30}$$

The derivative of induction time with respect to initial density is obtained by finite differences.

$$\left(\frac{\partial t_i}{\partial \rho_1} \right)_{T_1} \approx \frac{t_i(\rho_1 + \Delta \rho) - t_i(\rho_1)}{\Delta \rho} \; . \tag{31}$$

An example of the computation of an adiabatic, constant-volume explosion at an initial condition of 11 MPa and 1101 K is shown in Fig. 1. These initial conditions correspond to adiabatic compression ratio of 30 from initial state of 298.15 K and 101.325 kPa, for the compressed state and explosion parameters, see Table 1. This computation was carried out with the Shock and Detonation Toolbox routine demo_cv and the Hong et al. (2011) reaction mechanism.

The initial reaction process is dominated by high concentrations of the intermediate species H_2O_2 and HO_2 compared to the radicals H, O and OH until less than 1 μs before the sharp pressure rise at t_i = 0.13 ms associated with the consumption of the reactants. This is typical of low-temperature, high-pressure oxidation of hydrogen in which the three-body reactions dominate over the branching chain reactions in the initial stages of combustion. Once sufficient concentrations of intermediate species and radicals are created, the reactions involving these species results in the rapid increase in temperature and the dominance of the branching-chain process. The specific reactions and species that contribute to conversion of chemical to thermal energy are analyzed in Appendix C for the case shown in Fig. 1. Following the onset of significant energy release, the initial reaction process is then terminated by a coupled chain-branching thermal reaction, the concentrations of HO_2 and H_2O_2 rapidly drop and the reactants are almost completely consumed by the formation of H_2O. Following a brief excursion above equilibrium values, the concentrations of all species approaches the chemical equilibrium values appropriate to the constant-volume explosion temperature and pressure.

The rate-limiting step in the explosion process is the decomposition of H_2O_2,

$$H_2O_2 + M \longrightarrow 2\ OH + M \; ,$$

which has an activation energy of about 48 kcal/mol, comparable to the value obtained of 45 kcal/mol for the effective activation energy computed by perturbing the initial conditions.

For all of the cases of rapid compression ignition listed in Table 1, the progress of the reaction is similar. We illustrate the formation of HO_2 and H_2O_2 at early times (less than 5×10^{-6}) in the reaction pathway diagram for H and O atoms shown in Figure 2. The reaction pathways were computed using Cantera and the Python routine path.py. The initiation of consumption of HO_2 and H_2O_2, the development of the H, O and OH branching chain process and the generation of H_2O is illustrated in reaction pathway diagram for H and O atoms shown in Figure 5. Once the HO_2 and H_2O_2 concentrations are depleted, the branching chain reactions dominate the combustion process and the temperature quickly rises and the reaction rates increase correspondingly due to the generation of H_2O as illustrated in the reaction pathway diagram (Figure 6) for H and O atoms. Finally, the reactions quickly come to equilibrium following the complete consumption of reactants and the forward and reverse rates become equal with concentrations approaching equilibrium values consistent with the final temperature (4290.5 K) and pressure (35.2 MPa). This situation is shown in the reaction pathway diagram (Figure 7) for H and O atoms.

The variation of time-to-explosion with CR for five cases of initial pressure and temperature is illustrated in Figure 3. These values were computed with the program demo_cv_comp and the detailed chemical kinetic model and

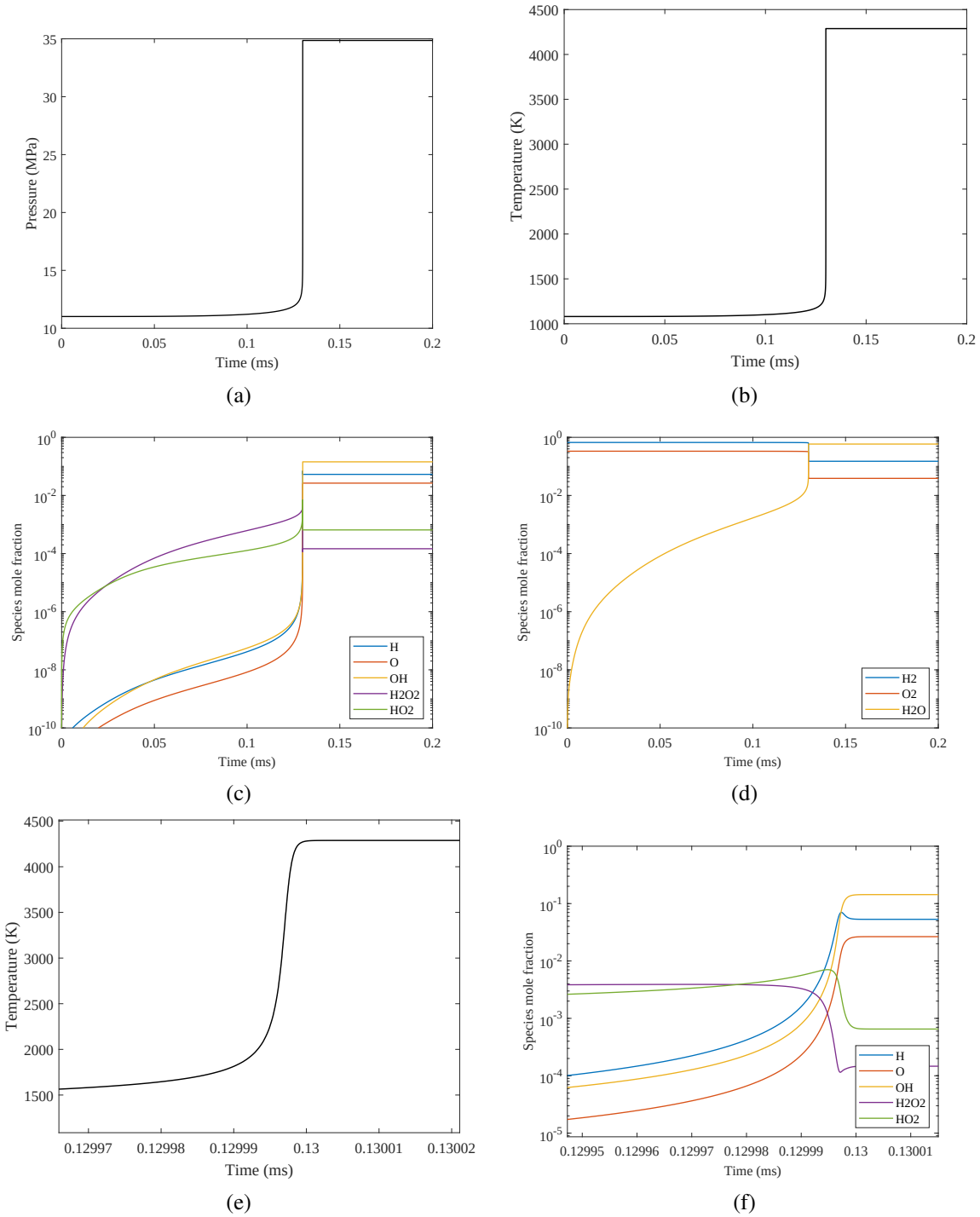

Figure 1: Adiabatic, constant-volume explosion of H_2-O_2 mixtures at 11 MPa and 1080 K (CR = 30 from standard initial conditions, P = 101.325 kPa, T = 298.15 K). Figures a, b, c, and d show the entire time evolution; e and f show only the 60 ns that brackets the explosive event at 0.13 ms.

thermodynamics of Hong et al. (2011). Values chosen are relevant to laboratory experiments (0.101 MPa, 298.15 K) and severe[3] accident conditions in nuclear power plants (0.101 to 6.86 MPa, 315-450 K). The effect of increasing

[3]A severe accident in a nuclear power plant involves a loss of the cooling capability that results in the overheating, oxidation (generating H_2)

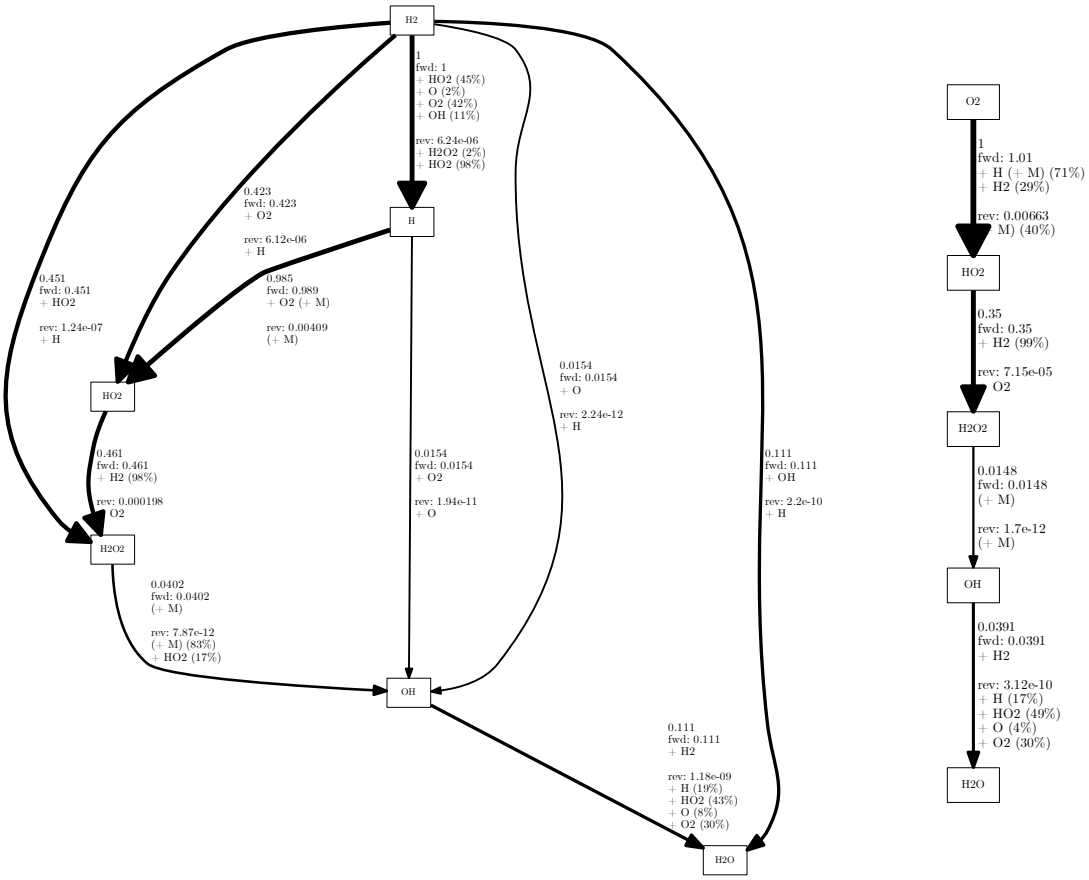

(a) (b)

Figure 2: Reaction pathways for (a) H atoms and (b) O atoms after adiabatic explosion of the case of Figure 1 at the very early stages with almost no reactant consumption, the temperature has only increased by 0.001 K and the time is $t = 4\times10^{-6}$ s, much less than the explosion time.

initial pressure or temperature is to decrease the induction time. In nuclear power plant severe accidents, there can be substantial steam in the combustible gas mixture, this also has an effect on the induction time as shown in Figure 4. The addition of steam increases the heat capacity and lowers the final temperature for a given compression ratio. Initial temperature increases result in much more dramatic changes in t_i^* than initial pressure changes due to substantial temperature sensitivity associated with the value of effective activation energy which is essentially identical for all of these cases (see the discussion in Section 5 and Figure 10). All of the data in Figures 3 and 4 can be collapsed to a universal relationship by representing the data in terms of the compressed gas temperature and density, see Figure 10.

From the results shown in Figures 2-7 and examining the quantitative values for the rates of creation and destruction for each species as well as the rates of progress for each reaction, the key reaction steps can be determined. The first H atoms are generated by the initiation reaction

$$H_2 + O_2 \longrightarrow H + HO_2 \,. \tag{R1}$$

The H atoms participate in the well known "shuffle" reactions to form the reactive oxygen atoms O and hydroxyl radicals OH

$$H + O_2 \longrightarrow OH + O \,, \tag{R2}$$

$$O + H_2 \longrightarrow OH + H \,. \tag{R3}$$

and melting of the reactor core. Severe accidents took place at TMI-2 (1979), Chernobyl (1986) and Fukushima (2011).

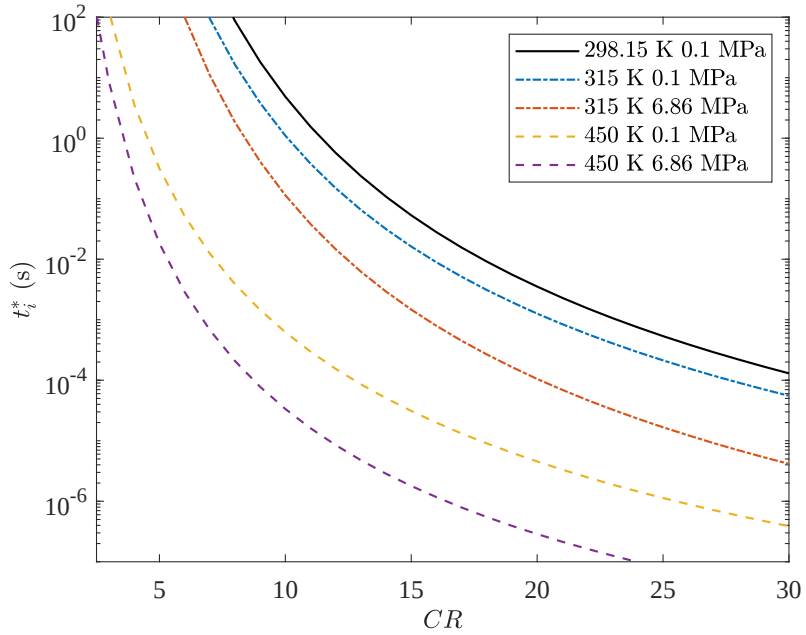

Figure 3: Adiabatic explosion time t_i^* as a function of compression ratio CR for five cases of initial temperature and pressure.

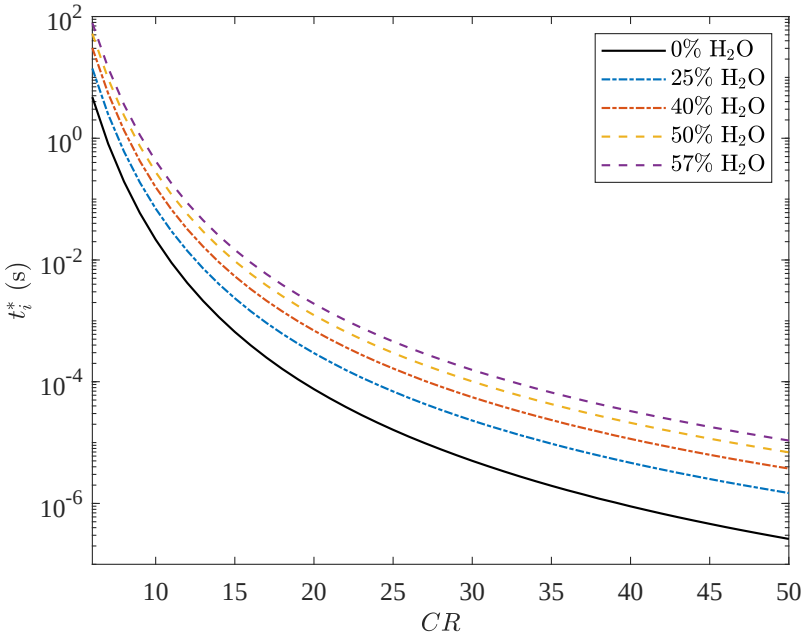

Figure 4: Adiabatic explosion time t_i^* as a function of compression ratio for five cases of stream diluted mixtures initially at 373.15 K and 0.1 MPa.

The OH radicals then produce an additional hydrogen atom, an essential species (the *chain carrier* in the high-temperature chain-branching process which is a key final step in hydrogen (and most hydrocarbon) explosive combustion processes

$$H_2 + OH \longrightarrow H + H_2O\ . \tag{R4}$$

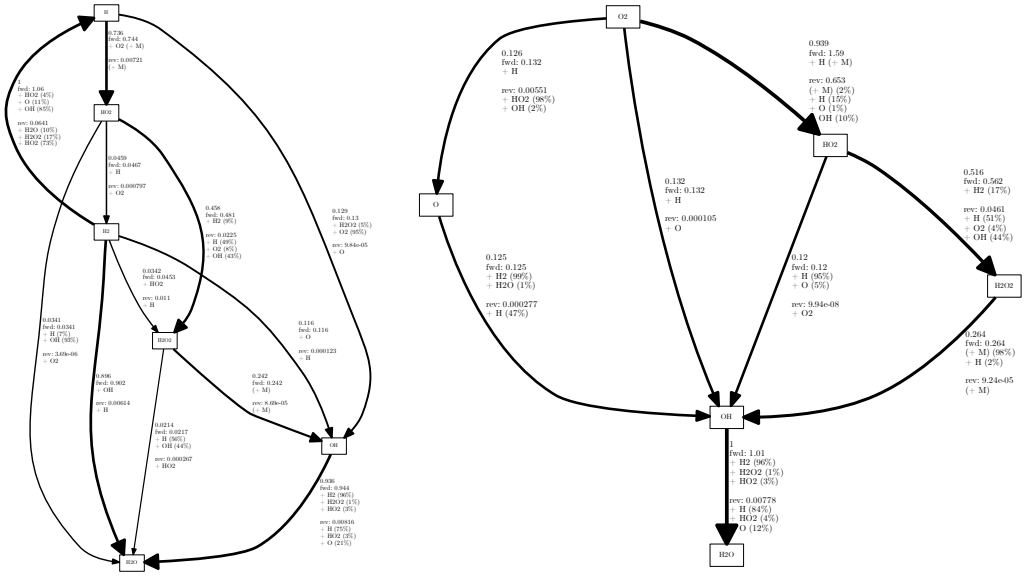

(a) (b)

Figure 5: Reaction pathways for (a) H atoms and (b) O atoms after adiabatic explosion of the case of Figure 1 has progressed to reach a temperature of 1600.0 K and immediately prior to the explosion time of 0.13 ms.

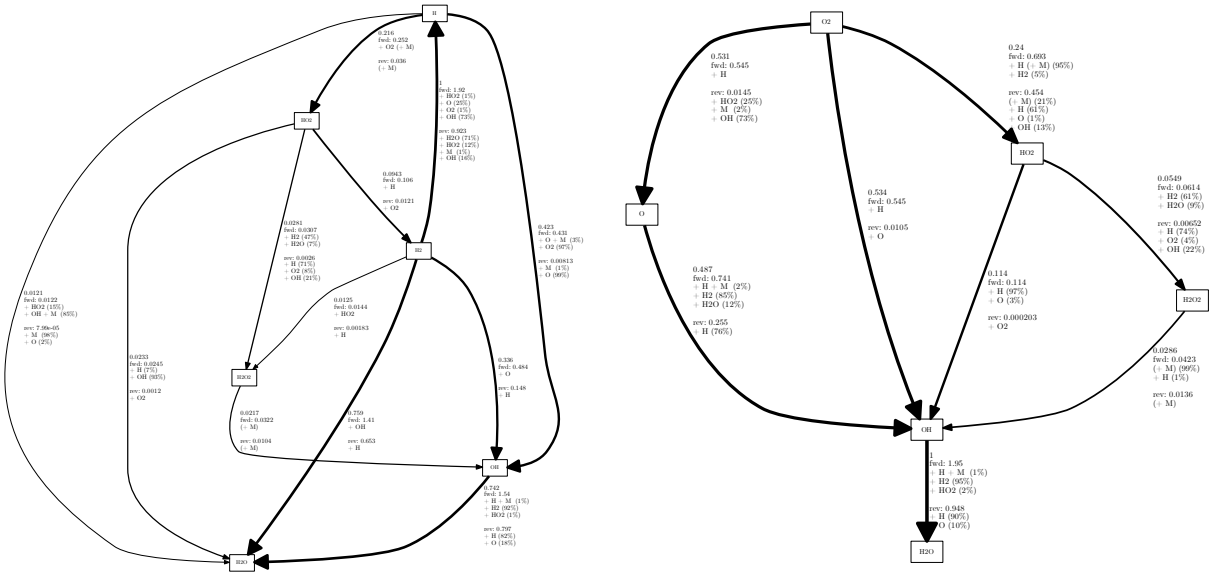

(a) (b)

Figure 6: Reaction pathways for (a) H atoms and (b) O atoms following adiabatic explosion of the case of Figure 1. after reactant consumption and the temperature has reached 3000 K and the time is close to the explosion time of 0.13 ms.

During the induction phase, the H atoms react with O_2 in the three-body reaction

$$H + O_2 + M \longrightarrow HO_2 + M\,, \tag{R5}$$

to a much greater extent than in R2 to produce the hydroperoxyl radical HO_2 which reacts to create hydrogen peroxide H_2O_2 through

$$HO_2 + H_2 \longrightarrow H_2O_2 + H\,, \tag{R6}$$

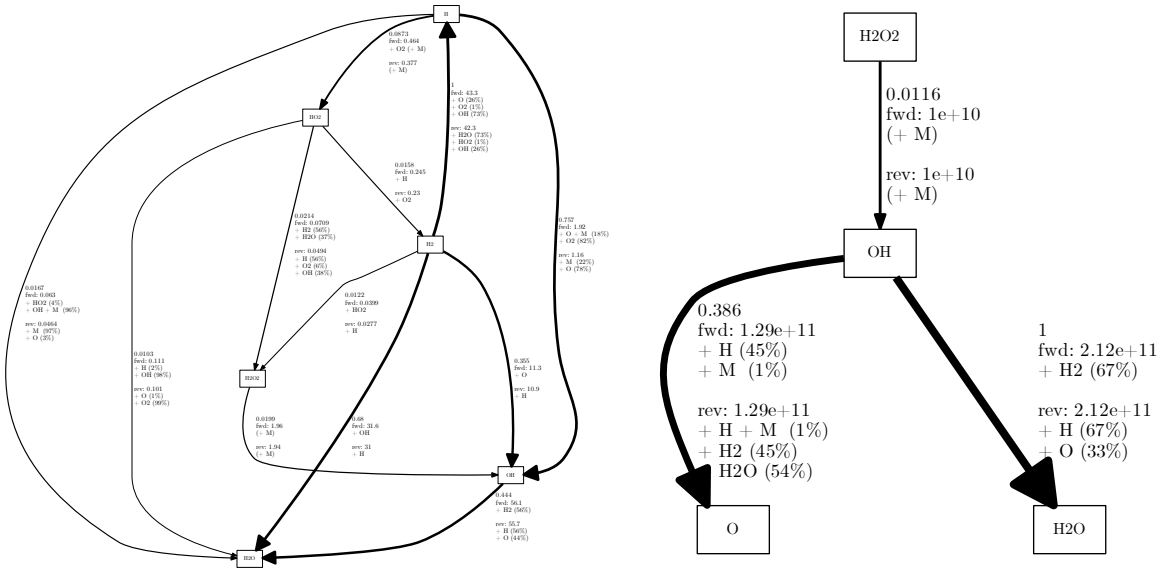

(a) (b)

Figure 7: Reaction pathways for (a) H atoms and (b) O atoms following adiabatic explosion of the case of Figure 1. The reactants have been consumed and the mixture is approaching equilibrium now that the branching chain reaction has ceased, the temperature has reached 4200 K and the time is just after the explosion time of 0.13 ms.

and

$$HO_2 + HO_2 \longrightarrow H_2O_2 + O_2 \,. \tag{R7}$$

Hydrogen peroxide slowly thermally decomposes to form hydroxyl radicals,

$$H_2O_2 + M \longrightarrow 2OH + M \,, \tag{R8}$$

which feed back into the chain-branching process through R4 to maintain the generation of H atoms. In the induction phase, the net generation rate of HO_2 and H_2O_2 through reactions R5, R6 and R7 substantially exceeds the destruction rates resulting in the buildup of concentrations for these two species until the rapid increase of temperature as well as concentrations of H, O and OH species during the chain-branching phase that terminates the explosion process. The much slower growth of the species O, H and OH during the induction phase occurs through the shuffle reactions R2, R3 and R4, which in concert with the other reactions involving these species results in the creation and destruction rates nearly being in balance, the so-called *quasi-steady state* condition.[4]

This is the simplest example of what Semenov (1959) refers to as *degenerate* branching[5], which has been extensively examined the context of low-temperature alkane (C_nH_{2n+2} denoted by RH) hydrocarbon oxidation. The accepted mechanism (Battin-Leclerc, 2008) of reaction is the abstraction of hydrogen (H) by molecular oxygen (O_2) or hydroxyl radicals ($\cdot$OH) leads to the formation of alkyl radical (C_nH_{2n+1} denoted by R$\cdot$), and through further reactions to form peroxy-alkyl ROO$\cdot$, and hydro-peroxy radicals $\cdot$OOH (HO_2) as well as alkyl-hydro-peroxides (ROOH). The O-O bond in the alkyl-hydro-peroxides is relatively weak and dissociation leads to the formation of RO$\cdot$ and $\cdot$OH, which provides positive feedback through further H-atom abstraction from the alkane; this is the essence of degenerative branching. In the case of alkanes and other hydrocarbons, isomerization of the peroxy-alkyl radicals creates hydro-peroxy-alkyl radicals (denoted $\cdot$QOOH) resulting in a sequence of reactions that generates additional $\cdot$OH radicals which contribute to the degenerate branching process as well as the formation of species such as cyclic ethers, aldehydes or ketones. In the case of hydrogen oxidation ($n = 1$), R = H and H_2O_2 plays the role of alkyl-hydro-peroxide species and no isomerization or further reactions will occur.

[4]These basic notions behind the chain reaction were developed in the 1920s by Hinselwood and Semenov, who also considered the extensions to treating the peroxide species (Semenov, 1959, Chap X and XII, Vol. 2) in the more general setting of low-temperature hydrocarbon oxidation.

[5]Also known as a straight chain mechanism

The reactions R1-R8 are all reversible but in the induction phase of the reaction, the reverse rates and the consumption of the reactants (H_2 and O_2) can be neglected. Applying the quasi-steady approximation to the rate equations for the H and OH species:

$$\frac{\mathrm{d}[\mathrm{O}]}{\mathrm{d}t} \approx 0 \ , \qquad \frac{\mathrm{d}[\mathrm{OH}]}{\mathrm{d}t} \approx 0 \ ; \tag{32}$$

the following algebraic relations are obtained:

$$[\mathrm{O}] = \frac{k_2[\mathrm{O}_2]}{k_3[\mathrm{H}_2]}[\mathrm{H}] \ , \tag{33}$$

$$[\mathrm{OH}] = \frac{2}{k_4[\mathrm{H}_2]} \left(k_2[\mathrm{H}][\mathrm{O}_2] + k_8[\mathrm{H}_2\mathrm{O}_2][\mathrm{M}]\right) \ . \tag{34}$$

Using these relationships in the rate equation for H, we obtain

$$\frac{\mathrm{d}}{\mathrm{d}t}[\mathrm{H}] = \left(\underbrace{2k_2[\mathrm{O}_2]}_{\text{chain branching}} - \underbrace{k_5[\mathrm{M}][\mathrm{O}_2]}_{\text{chain breaking}} \right) [\mathrm{H}] + \underbrace{2k_8[\mathrm{M}][\mathrm{H}_2\mathrm{O}_2] + k_6[\mathrm{H}_2][\mathrm{HO}_2]}_{\text{peroxide contributions}} + \underbrace{k_1[\mathrm{H}_2][\mathrm{O}_2]}_{\text{initiation}} \tag{35}$$

High-temperature and low pressure hydrogen-oxygen chain-branching explosions typically only consider reactions R1-R5. The role of the chain breaking reaction R5 is to slow down the growth of H atoms. Under these conditions, the contribution of reactions R6-R8 can be neglected and the hydrogen atom concentrations increase exponentially with time.

$$\frac{\mathrm{d}}{\mathrm{d}t}[\mathrm{H}] = \alpha[\mathrm{H}] + \beta \ , \tag{36}$$

which has the solution

$$[\mathrm{H}] = \frac{\beta}{\alpha} \left(\exp \alpha t - 1\right) \ , \tag{37}$$

where

$$\alpha = 2k_2[\mathrm{O}_2] - k_5[\mathrm{M}][\mathrm{O}_2] \ , \tag{38}$$

$$\beta = k_1[\mathrm{H}_2][\mathrm{O}_2] \ , \tag{39}$$

for positive values of α. Approximate models of this type have been considered by many researchers for interpreting shock tube Schott and Kinsey (1958), Skinner and Ringrose (1965), Brokaw (1965), Ripley and Gardiner (1966) and heated vessel explosion experiments Lewis and von Elbe (1961), Semenov (1959). These are usually referred to as *chain branching* explosions in which the explosive behavior is the exponential growth of the chain carrier H and the radicals O and OH through the quasi-steady state relationships (33) and (34). This behavior occurs even in isothermal conditions, which is a common assumption made to simplify analysis of the chemical reactions during the initial phase of the growth of radical species. Ultimately, in systems with a finite rate of heat transfer (often idealized as adiabatic for fast processes), the coupling of energy release and chemical reaction rates is an essential element of any realistic explosion process. At low-pressures and high-temperatures, the explosion process is often idealized as an isothermal induction period during which chain-branching dominates followed by brief exothermic transient in which radical species combine to form major reaction products.

The condition α = 0 is often referred to as the *crossover condition* as it represents a division between the dominance of chain branching involving only H, O and OH and the peroxide (HO_2 and H_2O_2) dominated induction period. This condition is also used to define the *second explosion limit* in vessel studies and extrapolation to higher pressures and temperature is referred to as the *extended second limit* in shock tube and detonation initiation Boeck et al. (2017) studies. In general, adiabatic explosion computations predict that for many fuels there is a shift in the reaction mechanism at a locus of $P-T$ conditions accompanied by a change in effective activation energy and reaction order Browne

et al. (Oct. 17-18, 2005), Liang et al. (2007). This effect is most pronounced for hydrogen oxidation and marked by a sharp peak in the effective activation energy in the vicinity of the extended second limit.

The usual criteria for the second limit or extensions is expressed as

$$2k_2 = k_5[\mathrm{M}] \tag{40}$$

where it is necessary to account for the pressure dependence and different collision efficiencies of the various third bodies M in the three-reaction R5. Many earlier studies considered that the competition for H atoms by R5 was *chain terminating* but at higher pressures, the reactions R6, R7 and R8 come into play and create a pathway for the creation of OH and re-establishment of chain branching.

At low-temperature and high-pressure (the case at maximum compression for all the conditions examined in our study) the rate of chain breaking exceeds the chain branching, $\alpha < 0$, and the rate of growth of HO_2 and H_2O_2 concentrations control the growth of H atom concentration, which are now in quasi-steady state because the rate of destruction is approximately equal to the rate of creation. Applying the quasi-steady approximation to the H atom rate equations yields

$$[\mathrm{H}] = \frac{2k_8[\mathrm{M}][\mathrm{H_2O_2}] + k_6[\mathrm{H_2}][\mathrm{HO_2}] + k_1[\mathrm{H_2}][\mathrm{O_2}]}{k_5[\mathrm{M}][\mathrm{O_2}] - 2k_2[\mathrm{O_2}]} \ . \tag{41}$$

The rate of production of peroxide species is controlled by two coupled ordinary differential equations

$$\frac{\mathrm{d}}{\mathrm{d}t}[\mathrm{HO_2}] = k_5[\mathrm{M}][\mathrm{O_2}][\mathrm{H}] - k_6[\mathrm{HO_2}][\mathrm{H_2}] - 2k_7[\mathrm{HO_2}]^2 \ , \tag{42}$$

$$\frac{\mathrm{d}}{\mathrm{d}t}[\mathrm{H_2O_2}] = k_7[\mathrm{HO_2}]^2 + k_6[\mathrm{HO_2}][\mathrm{H_2}] - k_8[\mathrm{H_2O_2}][\mathrm{M}] \ . \tag{43}$$

The role of HO_2 and H_2O_2 in vessel explosions at higher pressures was highlighted by Maas and Warnatz (1988) in their numerical study using a detailed chemical reaction mechanism, transport of species and energy to the vessel surface as well as surface reactions. More recent treatments (Sánchez et al., 2014, Liang and Law, 2018) of the predictions of limits in vessel explosions have conclusively shown the relevance of the H_2O_2 pathways in determining the boundaries between explosive and non-explosive behaviors.

The chemical reactions in the induction zone of detonations of lean hydrogen-air mixtures occur at high-pressure and moderate temperature conditions for which the HO_2 and H_2O_2 reaction pathways dominate as noted by Shepherd (1986) and explored through analytical modeling by Mikolaitis (1987). Fernández-Galisteo et al. (2009) analyzed lean ($0.25 < \phi < 0.5$) H_2-air flames at low pressure (1 atm) and concluded that it was possible to neglect H_2O_2 and by using the quasi-steady state approximation for H, O, OH and HO_2, they derived an explicit reaction rate for the effective one step reaction $2H_2 + O_2 \longrightarrow H_2O$ which could reproduce within 15% laminar burning speeds computed with detailed chemical kinetics.

Rapid compression machine testing has been used to extend ignition delay time measurements to high pressures (up to 7 MPa) at temperatures near the extended second limit (900-1050 K) where the HO_2 and H_2O_2 reaction pathways are expected to play a key role. Das et al. (2012) reviewed past studies and carried out experiments on stoichiometric H_2-O_2 mixtures diluted with various amount of N_2 and water vapor (H_2O(g)) as well as Ar at pressures between 10-70 MPa and temperatures from 900-1050 K. They determined that the mechanism of Hong et al. (2011) provided the closet predictions to the measured ignition delay times. From the modeling studies, Das et al. (2012) concluded that at low pressures, the ignition delay time increased with water vapor addition due the increased effectiveness of water as a third body in R5 inhibiting the growth of H atoms, while at the highest pressures tested, the addition of water vapor resulted in a decrease in induction time due the greater effectiveness in R8.

The RCM studies of Lee and Hochgreb (1998) using stoichiometric mixtures of H_2-O_2 diluted with Ar. Measurements of ignition delay time were preformed at temperatures between 950-1050 K and pressures up to 4 MPa. Predictions of ignition delay time with a detailed chemical reaction model were most sensitive to the rates of H_2O_2 formation and dissociation. As predicted by Kordylewski and Scott (1984), there is a significant amount of energy released during the induction period at high-pressure and low-temperature in contrast to the thermally-neutral induction process at low pressure and high temperature. Lee and Hochgreb (1998) identified the key reactions responsible for the non-isothermal behavior were R4 and R7, both exothermic and R8, endothermic. Net energy release is essential (Cain, 1986) to obtaining explosive reactions at high pressure, the thermal feedback accelerating the rate of R2 relative

to R8. Unlike the case of simple chain-branching, the reaction at high-pressure proceeds as a coupled chain-thermal explosion involving HO_2 and H_2O_2, leading to the generation of OH from H atoms with an effective overall reaction (Lee and Hochgreb, 1998) of

$$H + H + O_2 \longrightarrow OH + OH \quad .$$

Cain (1986, 1997) carried out experiments in a free-piston compression tube with H_2-O_2-He mixtures initially at 1-1.6 atm and found that ignition occurred at about 1150 K, relatively independent of the pressure at ignition, which was between 4-7 MPa. Cain's free piston compressor had shorter (4-7 ms) compression times than either Das et al. or Lee and Hochgreb (20-30 ms). Cain carried out numerical simulations based on a detailed reaction mechanism using an adiabatic model of the compression process to develop an analytical model to explain his results. Cain concluded that he could explain his results by considering the competition for H atoms as in the traditional second limit analysis and requiring that OH molecules reach a critical concentration for explosion to occur.

Although the reaction mechanism for hydrogen combustion has been well-established for several decades, refinements in the rate constants and comparison of model predictions with experimental data is an ongoing activity Olm et al. (2014), Konnov (2019) as well as the measurement of reaction rates at elevated pressures Hashemi et al. (2015). Although this may result in more accurate ignition delay times, the reaction pathways and qualitative understanding of ignition phenomena as a function of composition, pressure, and temperature appears to be mature.

4 Exponential Volume Change

The simplest case of volume expansion is to characterize the volume rate of change by a single time scale τ_e

$$\frac{1}{v}\frac{\mathrm{d}v}{\mathrm{d}t} = \frac{1}{\tau_e} \; . \tag{44}$$

If the time scale τ_e is a constant, then the volume time dependence can be obtained by simple integration

$$v(t) = v_1 \exp(t/\tau_e) \; , \tag{45}$$

and the energy equation can be expressed as

$$\frac{\mathrm{d}T}{\mathrm{d}t} = -\frac{1}{c_v}\sum_{i=1}^{k} e_i \frac{W_i \dot{\omega}_i}{\rho} - T\frac{R}{c_v}\frac{1}{\tau_e} \; . \tag{46}$$

If the rate of volume expansion is too large, i.e., τ_e is too small, the temperature increase due to reaction will be suppressed and eventually the temperature will decay with time rather than increase. In such a case, it is impossible to sustain a vigorous chain-branching process and the radical pool (H, O and OH) is never substantial enough to initiate the coupled chain-branching and thermal explosion. As a consequence, when the value of τ_e is less than some critical value τ_e^*, explosions are not observed. The existence of a critical decay rate was proposed in the context of detonation initiation (Eckett et al., 2000) and has been shown subsequently (Radulescu and Maxwell, 2010, Maxwell and Radulescu, 2011, Mével et al., 2019) to be broadly applicable to reacting flows with significant rates of volume change.

The critical decay rate effect is illustrated in Figure 8a for an instantaneously adiabatically-compressed mixture with a range of values of τ_e varying from ∞ to a value slightly less than the near critical value $\tau_e* \approx 0.996$ ms. This was computed with the program demo_cdr_exp and the Hong et al. (2011) reaction mechanism. The variation of induction time with decay time is shown in Figure 8b. The limiting value of τ_e^* is indicated by the vertical asymptote of induction time vs decay time as the limit is approached with decreasing τ_e. With increasing τ_e, the induction time approaches the asymptotic value t_i^* for constant-volume, adiabatic explosion with $\tau_e = \infty$. The effect of decay rate on the production of minor species is shown in Figure 9. For slightly subcritical values of the decay time, following a period of slow growth in the H, O and OH species and near static values of HO_2 and H_2O_2, the coupled chain-branching thermal explosion process reaches critical conditions and a rapid exothermic excursion occurs in Figure 9a. For slightly supercritical values of the decay time, very similar species profiles are observed until about 0.8 ms, after which the chain branching process stops and the H, O and OH as well as HO_2 decay and H_2O_2 maintains a constant value. The critical values of τ_e for adiabatically compressed H_2-O_2 mixtures with compression ratios between 15 and 50 are given in Table 1. The critical values were computed with the program demo_cdr_exp_critical and the Hong et al. (2011) reaction mechanism.

5 Analytical Model

An analytical model of the critical decay rate process can be developed using the methods of activation energy asymptotics (Buckmaster and Ludford, 1982, Kapila, 1983), following the methodology outlined in Eckett et al. (2000) for constant pressure explosion. An approximate one-step irreversible model of the reaction process is used for this method of analysis. If the mass fraction of products is Y, the reaction rate is given by

$$\frac{\mathrm{d}Y}{\mathrm{d}t} = A(1-Y)\exp(-E_a/\tilde{R}T) \; . \tag{47}$$

The pre-exponential factor A and the activation energy E_a are empirically determined constants chosen to fit the induction time temperature dependence for the mixture of interest. The internal energy is modeled as

$$e = c_v T - Y q \; , \tag{48}$$

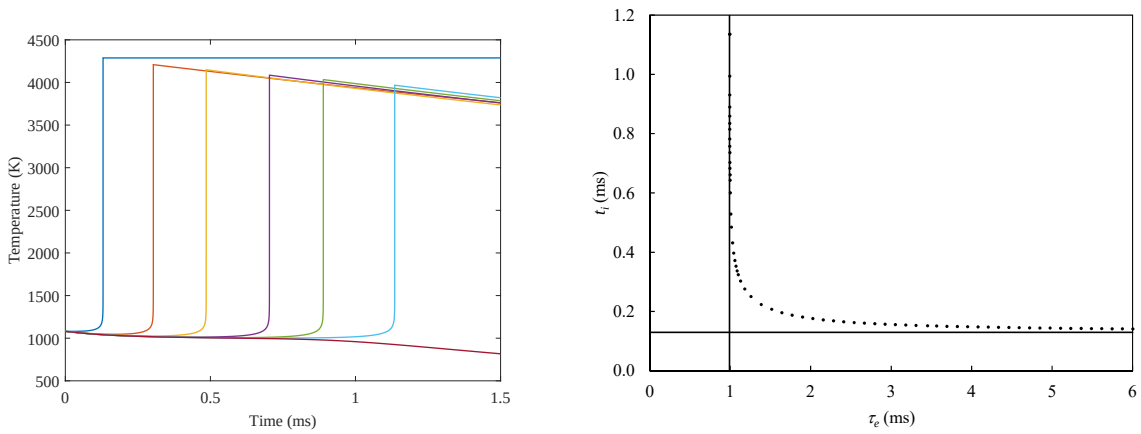

(a) (b)

Figure 8: (a) Temperature profiles for an explosion in an instantaneously adiabatically-compressed (CR = 30) stoichiometric H_2-O_2 mixture followed by an exponentially increasing volume characterized by an expansion time scale of τ_e = ∞, 1.128, 1.014, 0.9953, 0.9926, 0.9920, and 0.9915 ms (a completely quenched case). (b) Induction time t_i vs. expansion time τ_e the vertical asymptote corresponds the critical value τ_e^* and the horizontal asymptote corresponds to the induction time t_i^* ($\tau_e = \infty$) for a constant volume explosion.

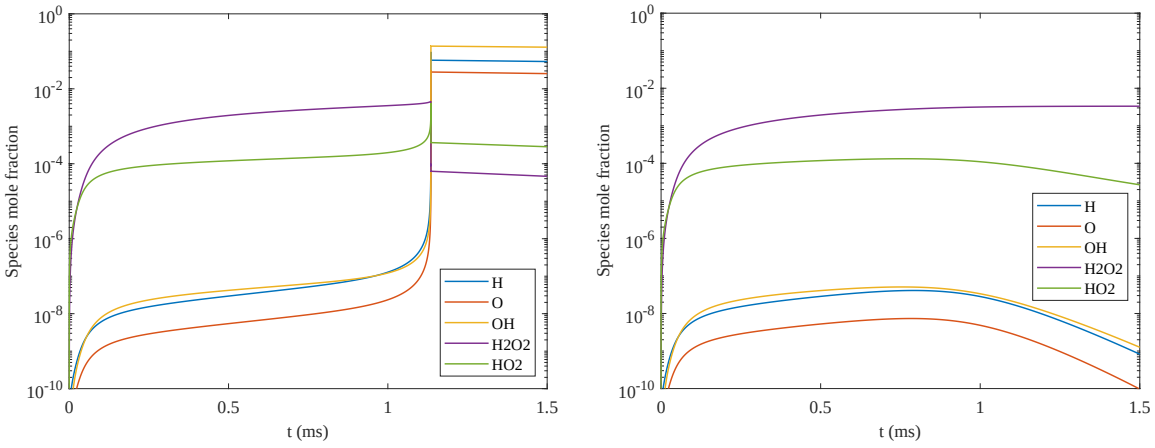

(a) (b)

Figure 9: Minor species for near-critical cases corresponding to Fig. 8 a) Initiation, τ_e = 0.9920 ms. b) Failure to initiate, τ_e = 0.9915 ms.

where the specific heat at constant volume c_v and specific energy of combustion q are emprically determined constants chosen to model the constant volume explosion conditions. Substituting this expression into the energy equation (1) the temperature equation is

$$c_v \frac{\mathrm{d}T}{\mathrm{d}t} = q\frac{\mathrm{d}Y}{\mathrm{d}t} - P\frac{\mathrm{d}V}{\mathrm{d}t} \ . \tag{49}$$

Substituting (47) for the reaction rate and using the ideal gas law $PV = RT$ to compute pressure, we have

$$c_v \frac{\mathrm{d}T}{\mathrm{d}t} = qA(1-Y)\exp(-E_a/\tilde{R}T) - RT\frac{1}{V}\frac{\mathrm{d}V}{\mathrm{d}t} \ . \tag{50}$$

Approximating the reaction consumption as negligible, $Y = 0$, the model equation for temperature is

$$\frac{\mathrm{d}T}{\mathrm{d}t} = \frac{qA}{c_v}\exp(-E_a/\tilde{R}T) - T\frac{R}{c_v}\frac{1}{v}\frac{\mathrm{d}v}{\mathrm{d}t} \ . \tag{51}$$

$$\tag{52}$$

The nondimensional activation energy is defined as

$$\theta = \frac{E_a}{\tilde{R}T_1} \ . \tag{53}$$

The method of activation energy asymptotics[6] presumes that for $\theta \gg 1$, the temperature variations are of order $O(1/\theta)$ during the induction period of the explosion and can be represented by the nondimensional variable ϕ defined by

$$\frac{T}{T_1} = 1 + \frac{\phi}{\theta} \quad \text{or} \quad \phi = \theta\frac{T-T_1}{T_1} \ . \tag{54}$$

and we can write

$$\frac{E_a}{\tilde{R}T} = \frac{\theta}{1+\dfrac{T-T_1}{T_1}} \ . \tag{55}$$

Expanding the denominator, we obtain

$$\frac{E_a}{\tilde{R}T} = \theta\left(1 - \frac{T-T_1}{T_1} + \left(\frac{T-T_1}{T_1}\right)^2 + \dots\right) \ , \tag{56}$$

$$= \theta - \phi + \frac{1}{\theta}\phi^2 + \dots \ , \tag{57}$$

and

$$\exp(-E_a/\tilde{R}T) = \exp(-\theta + \phi + \frac{1}{\theta}\phi^2 + \dots) \ . \tag{58}$$

Keeping only the first two terms of the expansion, we have the approximation

$$\exp(-E_a/\tilde{R}T) \approx \exp(-\theta + \phi) \ . \tag{59}$$

Further, we will characterize the rate of volume change by a time constant τ_e, defined as

$$\tau_e = \left(\frac{1}{V}\frac{\mathrm{d}V}{\mathrm{d}t}\right)^{-1} \ . \tag{60}$$

[6] A special feature of the activation energy asymptotics is to expand the argument of the Arrhenius factor but not the exponential function itself.

Substituting these last two expressions into (52), we obtain

$$\frac{\mathrm{d}\phi}{\mathrm{d}t} = \theta \frac{qA}{c_v T_1} e^{-\theta} e^{\phi} - \frac{R}{c_v} \frac{\theta}{\tau_e} \left(1 + \frac{\phi}{\theta} \right) \ . \tag{61}$$

In the limit of large activation energy, we require that

$$\lim_{\theta \to \infty} \theta e^{-\theta} \longrightarrow \text{constant} \ , \tag{62}$$

and

$$\lim_{\theta \to \infty} \theta \left(1 + \frac{\phi}{\theta} \right) \longrightarrow \theta \ . \tag{63}$$

The resulting equation for nondimensional temperature is

$$\frac{\mathrm{d}\phi}{\mathrm{d}t} = \theta \frac{qA}{c_v T_1} e^{-\theta} e^{\phi} - \frac{R}{c_v} \frac{\theta}{\tau_e} \ . \tag{64}$$

There are two special cases. First, consider the case of constant volume which is the limit of $\tau_e \to \infty$. Defining the constant volume induction time as

$$t_i^* = \frac{c_v T_1}{q \theta A} e^{\theta} \ , \tag{65}$$

and the nondimensional time as

$$\tilde{t} = \frac{t}{t_i^*} \ , \tag{66}$$

the temperature equation is

$$\frac{\mathrm{d}\phi}{\mathrm{d}\tilde{t}} = e^{\phi} \ . \tag{67}$$

This has the analytic solution

$$\phi = -\ln(1 - \tilde{t}) \ . \tag{68}$$

The result that $\phi \to \infty$ as $\tilde{t} \to 1$ is interpreted as defining t_i^* as the constant volume adiabatic explosion or ignition time. This result was first obtained by Todes in the 1930s (see Ch. IV Frank-Kamenetskii (1955) and Ch. VII, Vol. 2 Semenov (1959)) and continues to be used as guide to the interpretation of ignition experiments. Referring to Figure 4, we observe that the time-to-explosion computed with realistic thermochemistry and a detailed reaction mechanism is quite realistically represented for those cases by

$$t_i^* = a \exp(b/T) \ , \tag{69}$$

where a and b are constants which depend on the mixture initial conditions. The temperature dependence is consistent with the model solution with $b = E_a/\tilde{R} = 2.35 \times 10^4$, corresponding to an activation energy of 46.7 kcal·mol^{-1}. The parameter a takes on different values for different initial conditions because of the density dependence of the reaction rates, which is not accounted for in the simplest version (47) of the one-step reaction. If a factor ρ^n is included in the reaction rate expression

$$\frac{\mathrm{d}Y}{\mathrm{d}t} = A \rho^n (1 - Y) \exp(-E_a/\tilde{R}T) \ , \tag{70}$$

then the induction time expression will be

$$t_i^* = \rho^{-n} a \exp b/T \ , \tag{71}$$

where

$$a = \frac{c_v \tilde{R}}{q E_a A} \ , \qquad b = E_a/\tilde{R} \ . \tag{72}$$

For a given regime of reaction mechanism, a, n, and b are approximately constant as demonstrated in Figure 10. The values of these parameters was determined by linear regression of the logarithm of induction time against the variables $\ln \rho$ and $1/T$

$$\ln t_i^* = \ln a - n \ln \rho + b(1/T) \tag{73}$$

using the data set of 347 computed t_i^* values at the conditions shown in Figure 10. The results are n = 0.6276 $\pm$ 0.0075, a = 6.911 $\pm$ 0.35$\times 10^{-14}$ and b = 23067 $\pm$ 52. The value of n is consistent with the range of values (0.4 to 0.8) for the density dependence of the induction time computed according to (30) and the value of b is consistent with the computed range of effective activation temperatures according to (28).

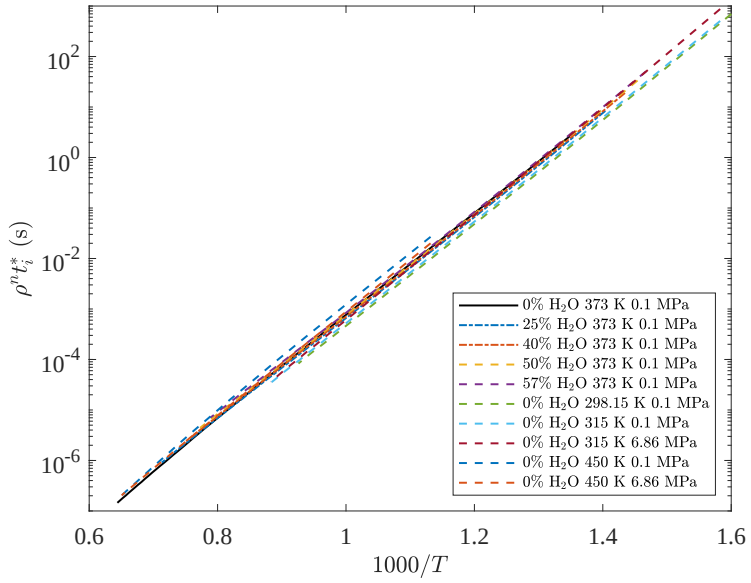

Figure 10: Arrhenius plot of scaled induction time vs. reciprocal temperature using the density exponent determined by linear regression.

Second, consider the case of finite τ_e and large θ. The temperature equation is approximately

$$\frac{\mathrm{d}\phi}{\mathrm{d}\tilde{t}} = e^{\phi} - (\gamma - 1)\theta \frac{t_i^*}{\tau_e} \ , \tag{74}$$

where we have assumed a perfect gas with

$$\gamma - 1 = R/c_v \ . \tag{75}$$

For a given mixture and decay time constant, we can integrate this equation in the form

$$\frac{\mathrm{d}\phi}{\mathrm{d}\tilde{t}} = e^{\phi} - \alpha \tag{76}$$

with

$$\alpha = (\gamma - 1)\theta \frac{t_i^*}{\tau_e} = \text{constant} \tag{77}$$

to obtain

$$\phi = -\ln[(1 - (1 - \alpha)e^{\alpha \tilde{t}})/\alpha] \tag{78}$$

This solution is identical to the one given by Eckett et al. (2000) in the context of blast wave initiation of detonation. There are three possible types of solutions depending on the value of α.
Case 1: Supercritical behavior, $\alpha < 1$. Ignition occurs at finite time, $\phi \to \infty$ as $\tilde{t} \to \tilde{t}^*$ where

$$\tilde{t}^* = \frac{1}{\alpha} \ln \frac{1}{1 - \alpha} \ . \tag{79}$$

Case 2: Critical behavior, α = 1. Ignition ($\phi \to \infty$) occurs only as $\tilde{t} \to \tilde{t}^*$. This is interpreted as defining the critical decay time constant by setting α =1 in (77)

$$\tau_e^* = (\gamma - 1)\theta t_i^* \ . \tag{80}$$

Case 3: Subcritical behavior, $\alpha > 1$. Ignition does not occur, $\phi \to -\infty$ as $\tilde{t} \to \infty$.

This model of an explosion only considers the thermal aspects and a realistic model of the explosion of a hydrogen-oxygen mixture under adiabatic compression has to consider the coupling of the chain-branching mechanism and the thermal energy release, as treated by the numerical simulations of the previous section. However, the general features of the temperature-time dependence and role of α in determining the course of the ignition process are qualitatively correct as shown in Figure 8. When the effective activation energy is determined by (28), the analytical expression (80) for critical decay time is surprising accurate, as shown by the comparison in Figure 15. Note that the critical decay time τ_e^* is approximately a factor of 10 larger than the constant volume ignition time t_i^* over a wide range of compression ratios (Table 1).

6 Rapid Compression Machines

A rapid compression machine (Goldsborough et al., 2017) or RCM is a single-stroke piston-cylinder mechanism that compresses a reactive mixture in 30-50 ms and holds the compressed mixture at the final volume until explosion occurs. Optical, temperature and pressure measurements are used to determine the progress of the chemical reaction. The simplest application is the measure the ignition time using dynamic pressure measurements to determine the interval between the end of the compression process and the onset of the explosion.

The simplest model (known as the "adiabatic core" model) of an RCM is to use variable volume adiabatic reactor described by (9) and (8). The V(t) is specified by measurements and the time derivative $\mathrm{d}V/\mathrm{d}t$ is obtained by smoothing and numerical differentiation. We have analyzed data[7] from Das et al. (2012) using this technique to validate the reaction mechanism Hong et al. (2011). Results of a validation study for six mechanisms using multiple data sets from the Sung laboratory RCM database are presented in Veilleux et al. (2019).

The volume and volume derivative data were interpolated for use in a variable volume adiabatic explosion simulation in the program demo_rcm. The thermodynamic properties and the detailed chemical kinetic model used were from Hong et al. (2011). Results for Das et al. Mixture No. 1 (12.5% H_2, 6.25% O_2, 81.25% N_2) at an initial temperature of 400 K and pressure of 0.233 MPa compressed to 6.95 MPa and 1009 K are shown in Figure 12. The compression ratio is 11.8 and the peak pressure and temperature occurs at 0.0351 s when the compression process ends. Heat transfer and crevice effects result in the slight decay of pressure and temperature following the end of the compression process.

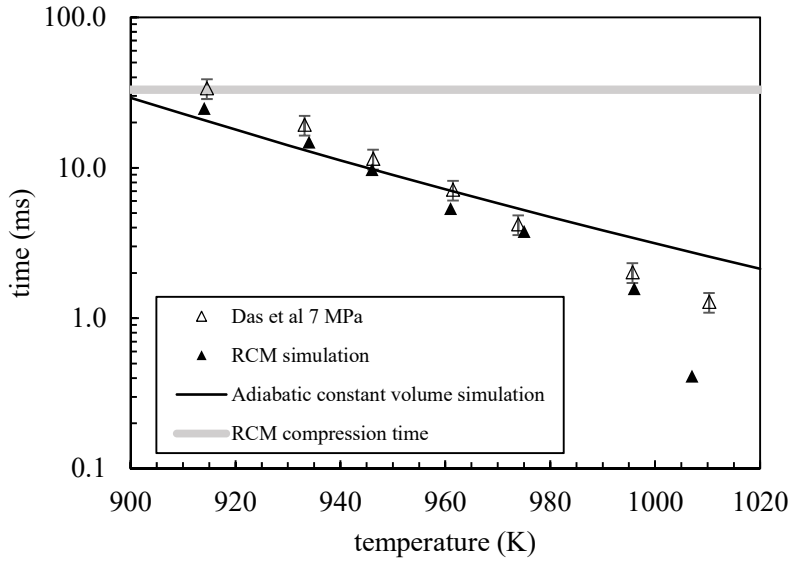

Figure 11: Analysis using Hong et al. (2011) reaction mechanism of Das et al. (2012) RCM data obtained at 7 MPa for Mixture No. 1.

This is a case with a rather short ignition delay (0.4 ms) and there is relatively little chemical reaction during the compression process and a small decay in pressure and temperature during the induction period. Accounting for both of these factors is much more important at lower temperatures and with longer induction periods. The results of analyzing the entire data set of Das et al. (2012) are shown in Figure 11. The measurements are in reasonable agreement with the modeling with the exception of the highest and lowest temperature conditions. At the lowest temperature, constant volume simulation and variable volume methods slightly underestimate the ignition delay time while at the highest temperature both method significantly overestimate the ignition delay time. There are significant uncertainties in measuring such short delay times from pressure data, a known limitation of RCM operation Goldsborough et al. (2017).

[7] Available for download from https://combdiaglab.engr.uconn.edu/database/rcm-database/

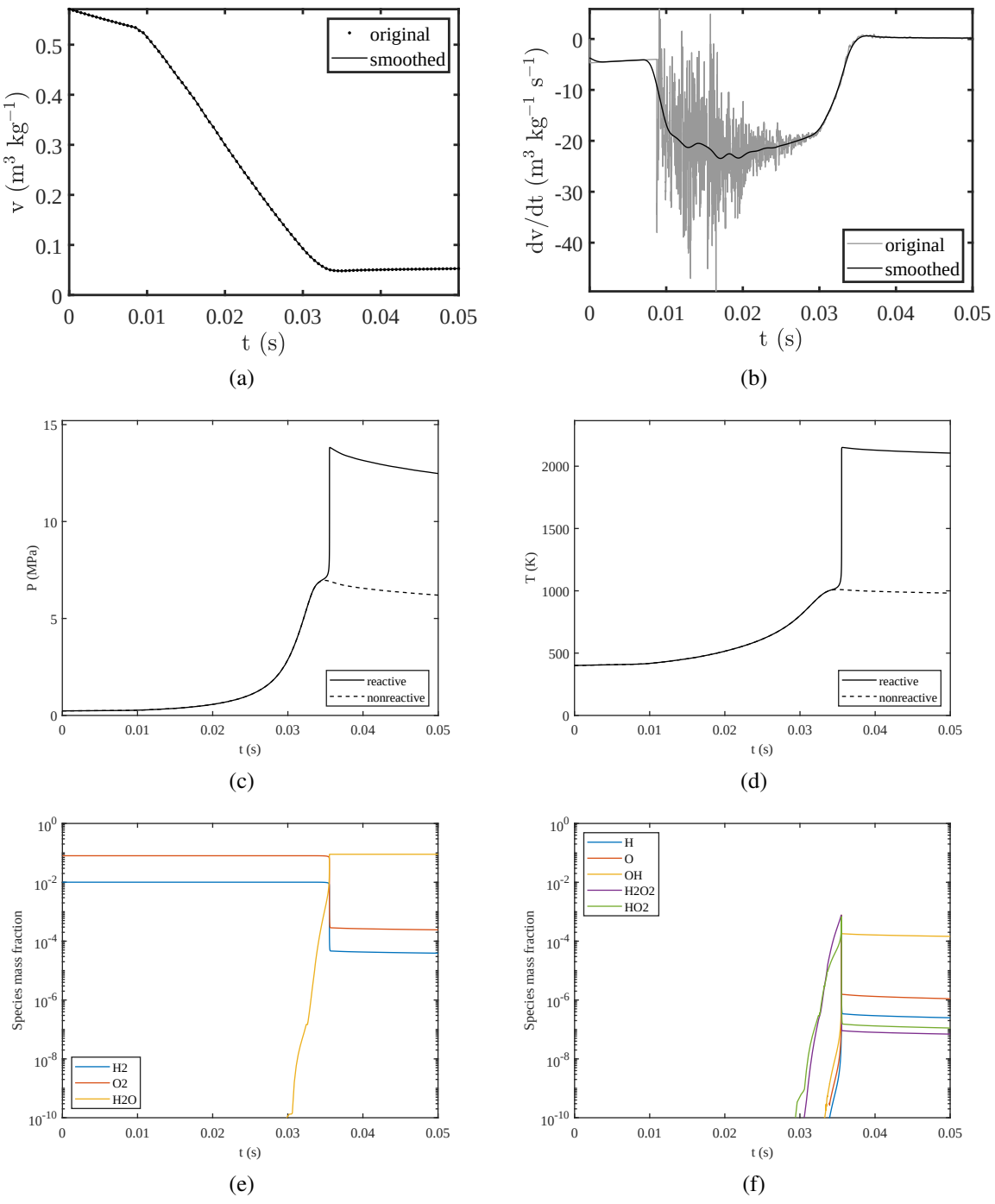

Figure 12: Analysis of Das et al. (2012) RCM data for Mixture 1 at an initial temperature of 400 K and pressure of 0.233 MPa. (a) volume - only every 50th data point is plotted; (b) volume time derivative; (c) pressure; (d) temperature; (e) major species; minor species.

7 Water Hammer

The volume transient in water hammer is combination of rapid compression followed immediately by rapid expansion (Coronel et al., 2020). As in the case of the rapid compression machine, the time to explosion will be a strong function of the compression ratio. However, unlike the typical rapid compression machine, the expansion following compression is significant and the ability to initiate and sustain an explosion will depend on the expansion rate being less than a critical value.

Based on water hammer testing carried out in our laboratories (Coronel et al., 2020, Veilleux et al., 2019), we have proposed an approximate analytical model for the volume change as a function of time that mimics both the rapid compression and expansion phases. This model is based on using a Gaussian function of time

$$V(t) = A\exp(-(t-t_m)^2/\tau_v^2) + B \ , \tag{81}$$

where the constants A and B are determined by the initial volume $V(0) = V_0$, and the minimum volume $V(t_m) = V_m$. The time of minimum volume t_m is arbitrary and the pulse width τ_v is selected to have values relevant to the water hammer case of interest.

$$V_o = A\exp(-t_m^2/\tau_v^2) + B \ , \tag{82}$$

$$V_m = A + B \ . \tag{83}$$

Solving for the constants and substituting in the original expression, we obtain

$$V(t) = (V_o - V_m)\left[\frac{1-\exp(-(t-t_m)^2/\tau_v^2)}{1-\exp(-t_m^2/\tau_v^2)}\right] + V_m \ . \tag{84}$$

The expression for normalized volume as a function of time can be written in terms of the *compression ratio* $CR = V_o/V_m$

$$\frac{V}{V_o} = \left(1-\frac{1}{CR}\right)\left[\frac{1-\exp(-(t-t_m)^2/\tau_v^2)}{1-\exp(-t_m^2/\tau_v^2)}\right] + \frac{1}{CR} \ . \tag{85}$$

For computational purposes, t_m is chosen to be a multiple of τ_v so that V is sufficiently close to V_o at $t = 0$. In practice a value of $t_m = 3\tau_v$ is adequately large. The total duration of a numerical simulation for the purpose of determining critical pulse length was selected to be $6\tau_v$ after a series of trial computations. The time derivative of the volume required as input to the energy equation can be computed analytically.

$$\frac{\mathrm{d}}{\mathrm{d}t}\left(\frac{V}{V_o}\right) = \left(1-\frac{1}{CR}\right)\left[\frac{\exp(-(t-t_m)^2/\tau_v^2)}{1-\exp(-t_m^2/\tau_v^2)}\right]\frac{2(t-t_m)}{\tau_v^2} \tag{86}$$

7.1 Interpretation of Pulse Width

The parameter τ_v is proportional to the half-width $\tau_{v,1/2}$ of the volume pulse

$$V(t_m + \tau_{v,1/2}) = \frac{1}{2}(V_o + V_m) \ . \tag{87}$$

For the parameters used in the present study, the volume pulse half-width can be computed from (85) to be

$$\tau_{v,1/2} \approx (\ln 2)^{1/2}\,\tau_v \ , \tag{88}$$

$$= 0.832\,\tau_v \ . \tag{89}$$

The corresponding half-width of the ideal pressure pulse $\tau_{p,1/2}$ at one-half maximum pressure is substantially smaller than $\tau_{v,1/2}$ due the insentropic relationship between P and V, as illustrated in Fig 13. Assuming a constant ratio of specific heats γ, the pressure half-width can be computed using the approximate isentrope

$$\frac{P}{P_o} = \left(\frac{V}{V_o}\right)^{-\gamma} \ , \tag{90}$$

to be

$$\tau_{p,1/2} = \left[\ln\left(\frac{CR-1}{CR-2^{1/\gamma}}\right)\right]^{1/2} \tag{91}$$

$$\approx \left(\frac{2^{1/\gamma}-1}{CR}\right)^{1/2} \tau_v \ . \tag{92}$$

For a nominal value of γ = 1.4 and a compression ratio of 15, this is numerically

$$\tau_{p,1/2} \approx 0.20\,\tau_v \ . \tag{93}$$

The constant of proportionality decreases with increasing CR and at CR = 60

$$\tau_{p,1/2} \approx 0.10\,\tau_v \ . \tag{94}$$

This substantial difference between the pressure and volume pulse half-widths is important in evaluating test results from experimental pressure measurements.

An example of a computation with a near-critical pulse width parameter τ_v = 1.07 ms for CR = 30 is illustrated in Figure 13 and 14. This computation was carried out with the program demo_pulse_cdr of the Shock and Detonation Toolbox. The thermodynamic properties and the detailed chemical kinetic model used were from Hong et al. (2011). For the near-critical cases, ignition occurs after the compression peak and during the expansion phase of the volume. For the temperature and pressure histories in Figure 13c and d, the nonreactive case is shown on the same plot. The competition between energy release and expansion work in the near-critical case results in a nearly constant temperature history after the compression peak until explosion. On the other hand, the pressure begins to drop immediately after the compression peak until the ignition takes place. The species profiles (Figure 14) show a very similar behavior as in the constant volume or exponential volume expansion cases with HO_2 and H_2O_2 dominating the concentrations until immediately before the branching chain explosion that results in the consumption of those species and ultimately, the reactants.

The existence of the critical pulse width parameter can be explained by the competition between chemical reaction energy release and work done by the expansion following the compression peak as discussed in Section 4. However, the characteristic expansion time τ_e is not a constant but varies during the volume expansion phase. First, we consider the variation of $dV(t)/dt$. The peak value of the derivative of volume with time is

$$\left(\frac{\mathrm{d}V}{\mathrm{d}t}\right)_{max} = \frac{1}{\tau_v}\sqrt{\frac{2}{e}}\,(V_o - V_m) \approx 0.858\,\frac{V_o - V_m}{\tau_v} \tag{95}$$

and this occurs at a time $t = t_m + \tau_v/\sqrt{2}$.

Second we consider the analog of τ_e as defined in (44) as a function of time

$$\tau_v(t) = \left(\frac{1}{V}\frac{\mathrm{d}V}{\mathrm{d}t}\right)^{-1} \ . \tag{96}$$

Based on our previous experience with the critical decay model, we expect that the quenching effect of the volume expansion will be dominated by the most rapid expansion rate or equivalently, the smallest value of $\tau_v(t)$ during the expansion phase $t > t_m$. Analytical computations using the model of (85) and (86) shows that (96) reaches a local minimum at $t - t_m \approx \tau_v/\sqrt{CR}$ and has the value

$$\left(\frac{1}{V}\frac{\mathrm{d}V}{\mathrm{d}t}\right)^{-1}_{min} = \tau_{v,min} \approx \frac{\tau_v}{\sqrt{CR}} \ . \tag{97}$$

As a consequence, the minimum characteristic decay time $\tau_{v,min}$ for the Gaussian pulse model can be substantially smaller than the pulse width parameter. For CR = 15, $\tau_{v,min}$ = 0.26 τ_v and for CR = 60, $\tau_{v,min}$ = 0.13 τ_v.

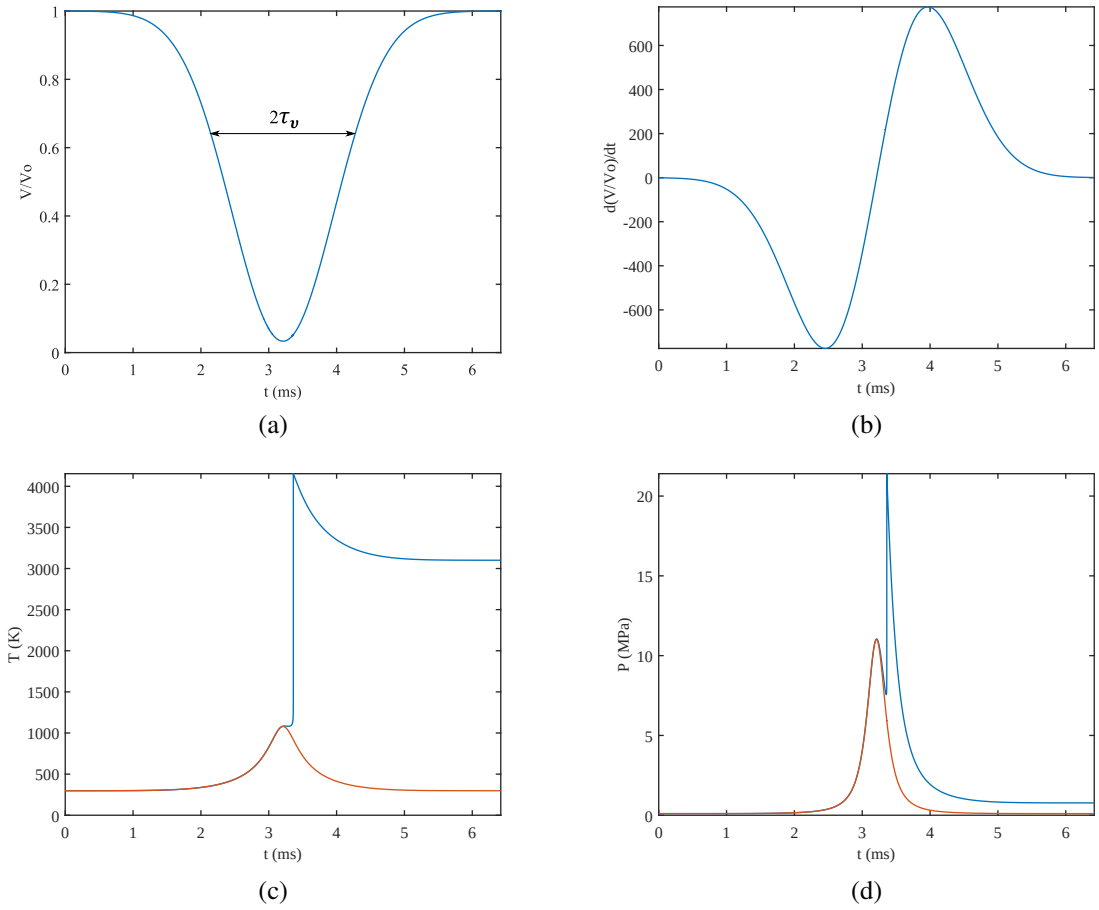

Figure 13: Normalized volume(a), volume time derivative (b), temperature (c) and pressure (d) for a near-critical (τ_v = 1.07 ms) ignition case for Gaussian volume pulse compression with CR = 30. Stoichiometric H_2-O_2 mixture initially at 298.15 K and 101.325 kPa.

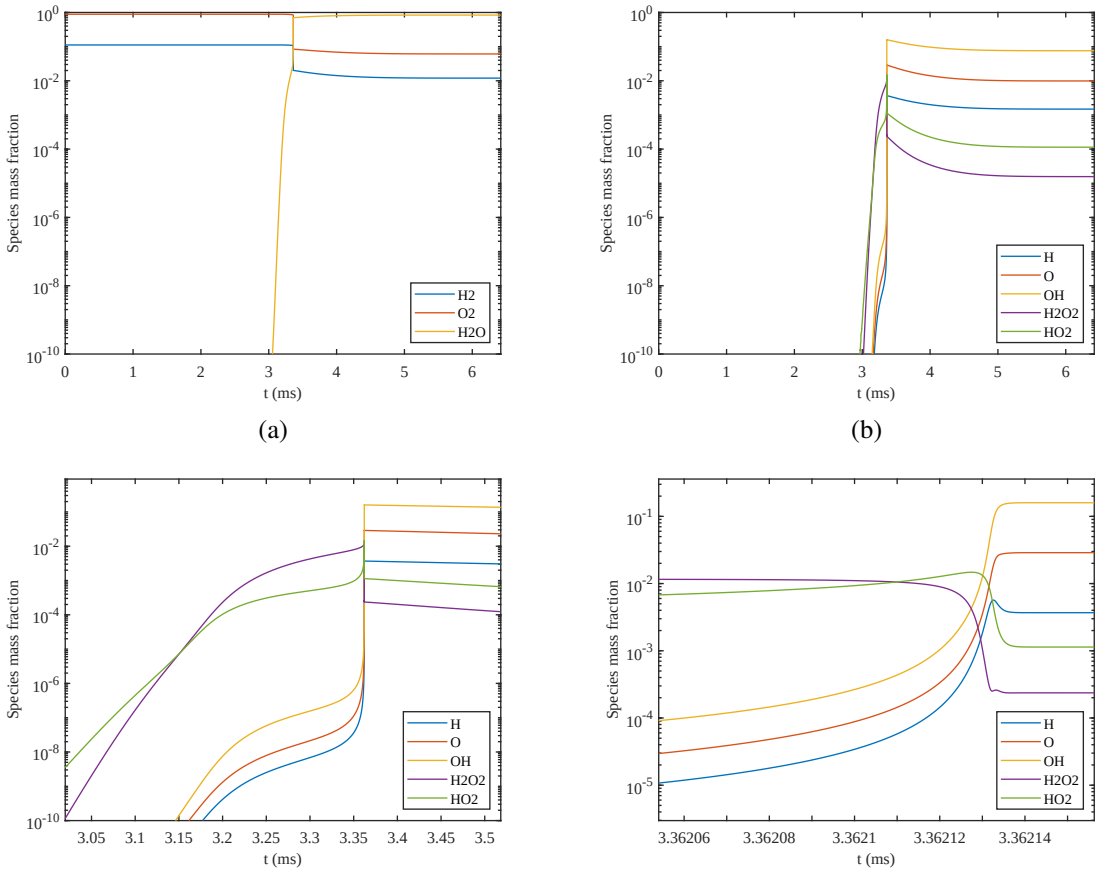

Figure 14: Major (a) and minor species (b(, (c), (d) for near-critical (τ_v = 1.07 ms) ignition case for Gaussian volume pulse compression with CR = 30. Stoichiometric H_2-O_2 mixture initially at 298.15 K and 101.325 kPa.

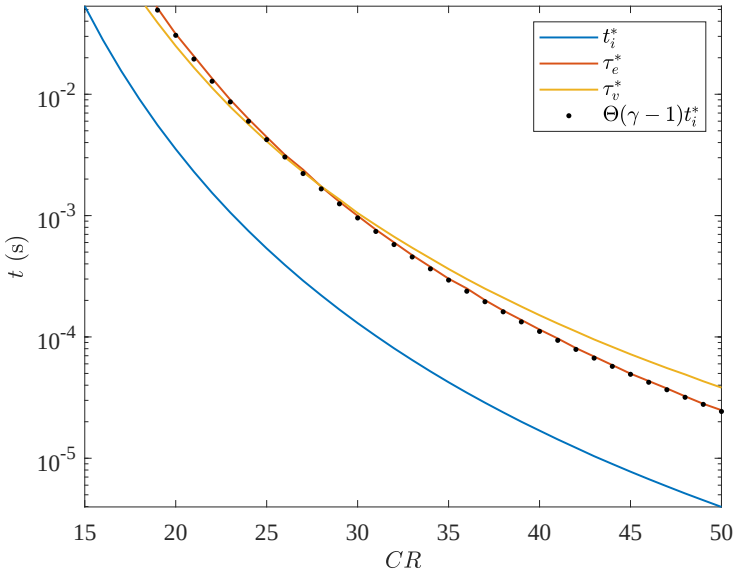

Figure 15: Comparison of four time scales for models of adiabatic explosions for a stoichiometric H_2-O_2 mixture initially at 298.15 K and 101.325 kPa.

7.2 Effect of CR and Initial conditions

We have used this model to compute the relationship between the critical pulse width parameter τ_v^* for ignition to occur as a function of the compression ratio CR for stoichiometric H_2-O_2 mixtures. This computation was carried out with the program demo_pulse_tau_critical of the Shock and Detonation Toolbox. The thermodynamic properties and the detailed chemical kinetic model used were from Hong et al. (2011).

The results are shown in Fig. 15 and Table 1. The closeness of the critical pulse width parameter and critical decay time can be observed in both the table and graph. This striking coincidence suggests that of all the time scales associated with the Gaussian pulse, the critical time scale defined by the peak volume derivative (95), which can be expressed as

$$\tau^* = \frac{V_o - V_m}{\left(\dfrac{\mathrm{d}V}{\mathrm{d}t}\right)_{max}} \approx 1.16\,\tau_v^* \tag{98}$$

most closely corresponds to τ_e^* of the exponential decay model.

For a given compression ratio, increasing the initial temperature decreases the induction time and the critical pulse width. On the other hand, adding steam to the mixture increases the induction time and critical pulse width. Results are shown for stoichiometric H_2-O_2 mixtures with 0, 10, 20 and 30% (vol) steam concentrations for three initial temperatures in Figures 16 and 17. At a given compression ratio, the addition of 30% steam increases the critical pulse width by almost an order of magnitude over undiluted mixtures. This is consistent with the comparable increase in adiabatic explosion time with the addition of water vapor that is shown in Figure 4. The effect of initial temperature is shown in Figure 17. At a given value of CR, increasing the initial temperature from 315 to 450 K for an initial pressure of 6.86 MPa results in a decrease in the critical pulse width of approximately two orders of magnitude. The magnitude of this effect is comparable to the reduction in adiabatic explosion time shown in Figure 3.

Experiments on water hammer ignition (Coronel et al., 2020, Veilleux et al., 2019) used N_2 dilution as a surrogate for steam because the tests were carried out at room temperature initial conditions. The effect of increasing nitrogen dilution, shown in Fig. 19, is to uniformly increase both t_i^* and τ_v^* over the range of CR studied. At a given value of CR, the ratios of induction and critical pulse times for a diluted mixture to those of an undiluted mixture are approximately constant. A dilution of 25% N_2 increases the time scales t_i^* and τ_v^* by a factor of 1.2 to 1.3, a dilution of 50% N_2 increases the time scales by a factor of 1.7 to 2.0 over the undiluted cases. Dilution by steam has a stronger effect on the time scales than nitrogen because H_2O is much more effective as a third-body than N_2 in the chain-breaking reaction (R5). An alternative to using N_2 as simulant for steam is a mixture of CO_2/He (in molar ratio

of 60/40) which was proposed by Lamoureux et al. (2003). As shown in Appendix B, at 50% dilution, the CO_2/He mixtures result in a close match for pressure (Fig. 21), temperature (Fig. 22) and adiabatic explosion time (Fig. 23) over the range $15 < CR < 60$. By comparison, N_2 dilution results in substantial higher temperatures and pressures at the same CR and consequently adiabatic explosion times t_i^* which are an order of magnitude lower. This effect is primarily due to the much higher heat capacity of the steam and CO_2/He simulant in comparison to N_2.

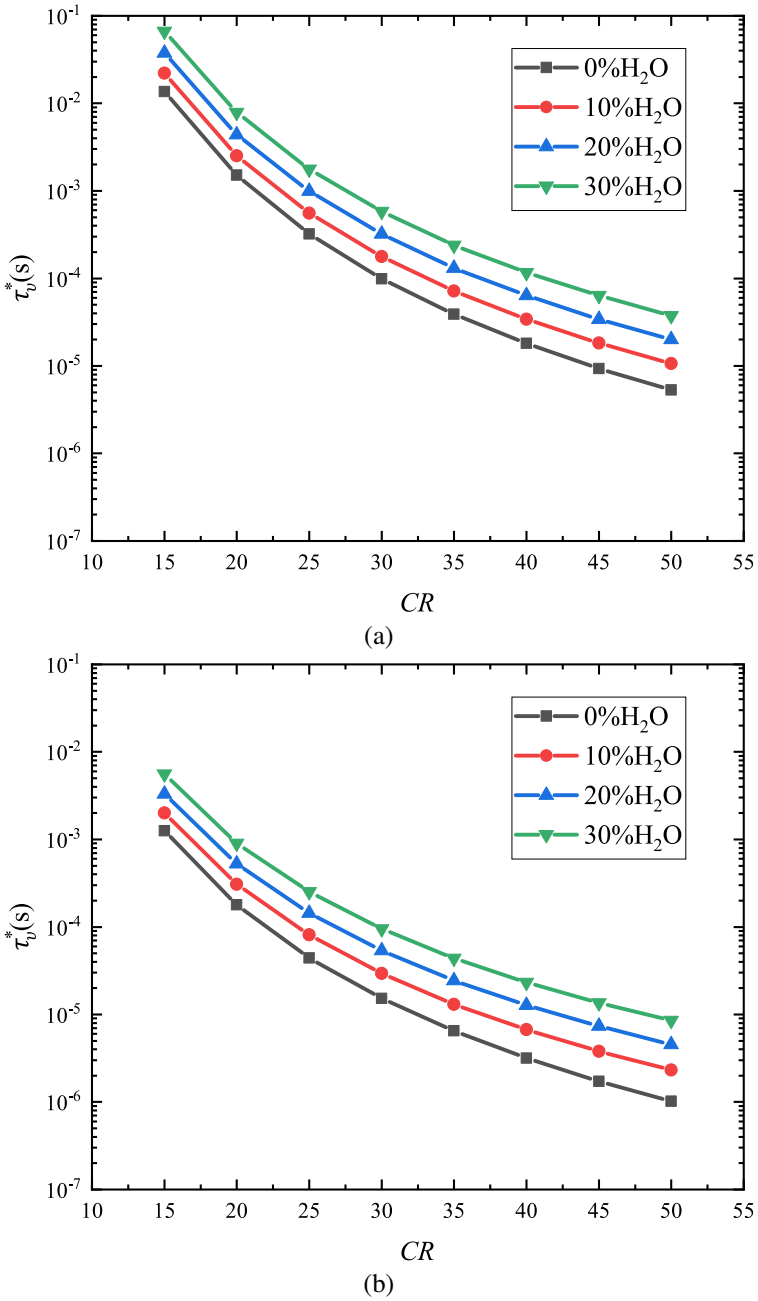

Figure 16: Effect of steam (H_2O(g)) concentration on critical pulse width for adiabatic explosion initiation of stoichiometric H_2-O_2 mixtures with a Gaussian pulse of volume compression. a) 348.15 K and 101.325 kPa initial conditions. b) 398.15 K and 101.325 kPa MPa initial conditions.

The analysis of experimental water hammer data (Coronel et al., 2020, Veilleux et al., 2019) is best based on pressure histories as the accurate direct measurement of volume histories is challenging. Either experimental or model pressure histories $P(t)$ can be used in simulations based on integrating the energy (11) and species (8) equations with

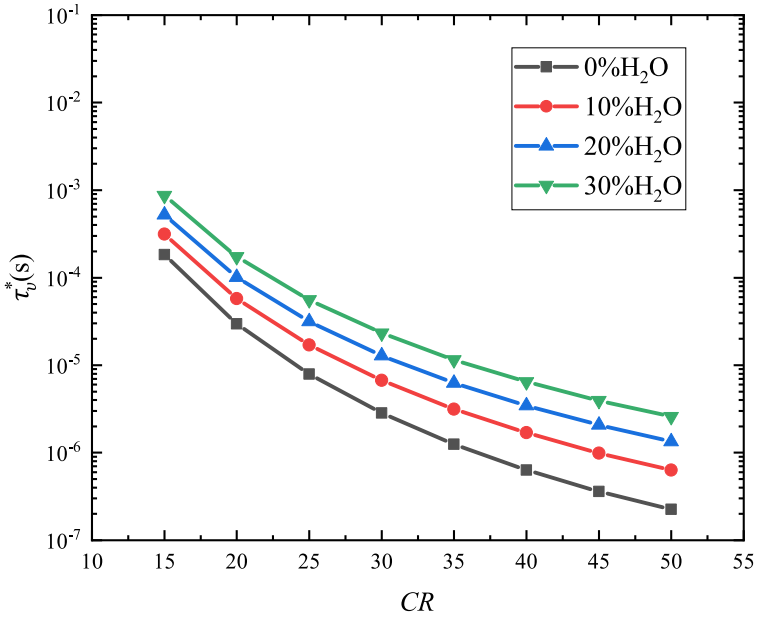

Figure 17: Effect of steam (H_2O(g)) concentration on critical pulse width for adiabatic explosion initiation of stoichiometric H_2-O_2 mixtures with a Gaussian pulse of volume compression. a) 448.15 K and 101.325 kPa initial conditions.

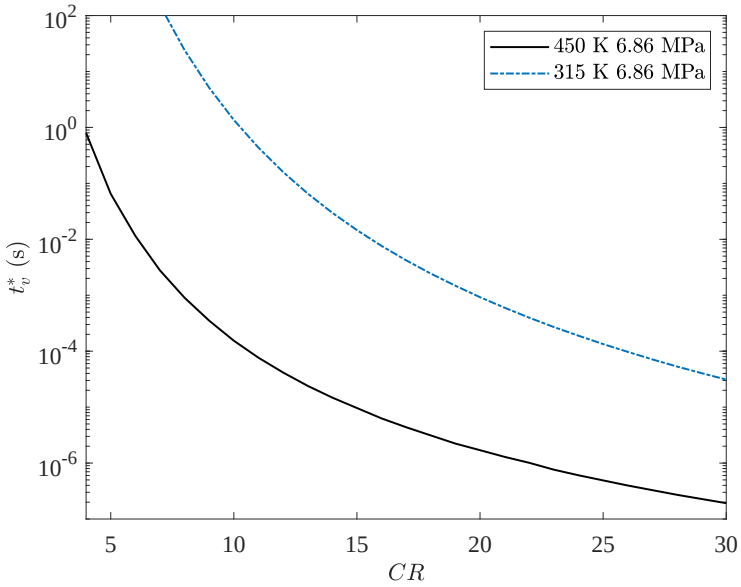

Figure 18: Effect of compression ratio on critical pulse width parameter for adiabatic explosion initiation of stoichiometric H_2-O_2 mixtures with a Gaussian pulse of volume compression; The initial pressure was 6.86 MPa for the two initial temperatures of 315 and 450 K.

a detailed chemical reaction network. Although the constraint of specified pressure is not as physically realistic as specified volume, the goal of such simulations is to evaluate ignition thresholds as a function of pressure history rather than following the full time evolution of the system. In fact, in water-hammer transients, the gas pressure and volume are coupled through the dynamics of the surrounding liquid and specifying $P(t)$ or $V(t)$ is an imperfect but useful approximation during the explosion phase.

As an example, we have simulated the water hammer experiments of Coronel et al. (2020), Veilleux et al. (2019)

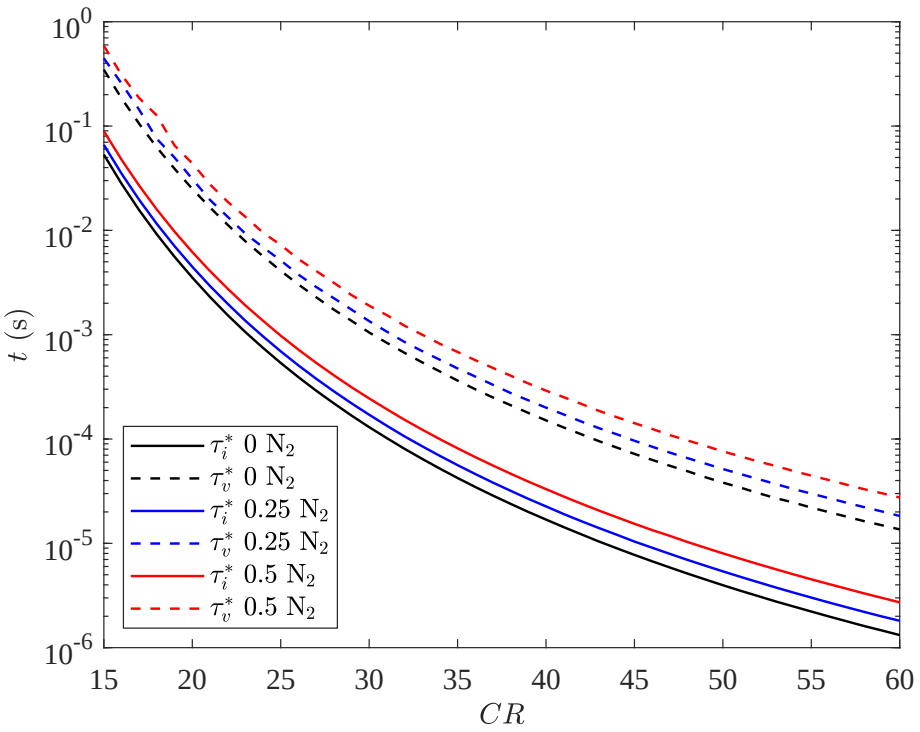

Figure 19: Induction time t_i^* and critical volume pulse width parameter τ_v^* for a Gaussian pulse of volume compression as a function of the peak compression ratio CR.

using the model pressure profile

$$P(t) = (P_m - P_o)\exp(-(t - t_m)^2/\tau_p^2) + P_o \tag{99}$$

where t_m, P_m and τ are parameters chosen to bracket the observed experimental pressure pulses. For a given value of P_m, there is a critical value τ_p^*; this is the analog of the critical value t_v^* found for the volume compression pulses. Explosive behavior is found for $\tau_p > \tau_p^*$ and non-explosive behavior occurs for $\tau_p < \tau_p^*$. Because pressure is specified, the determination of τ_p^* must be made by determining the values of τ_p that separate explosive temperature rise from essentially inert behavior. Examples of solutions for τ_p^* as a function of P_m are shown in Fig. 20 for a subset of the cases reported in Fig. 19

The results in Fig 20 can be compared to those in Fig. 19 using the methodology mentioned at the end of Section 7.1. To complete the connection between the pressure and volume pulse characteristics, we note that pressure pulse half-width considered earlier can be related to the pressure pulse parameter by

$$\tau_{p,1/2} = (\ln 2)^{1/2}\,\tau_p \tag{100}$$

so that the pressure and volume pulse parameters are related by

$$\tau_p \approx \left[\frac{2^{1\gamma} - 1}{CR\ln 2}\right]^{1/2} \tau_v \tag{101}$$

For example, for a peak pressure of 15 MPa, τ_p^* = 33, 44, 62 μs for 0, 25 and 50% N_2 dilution and the corresponding estimated values based on (101) and directly computed values of τ_v^* are 34.5, 45, and 66. A similar level of agreement is found for other peak pressures over the range shown in Fig. 20.

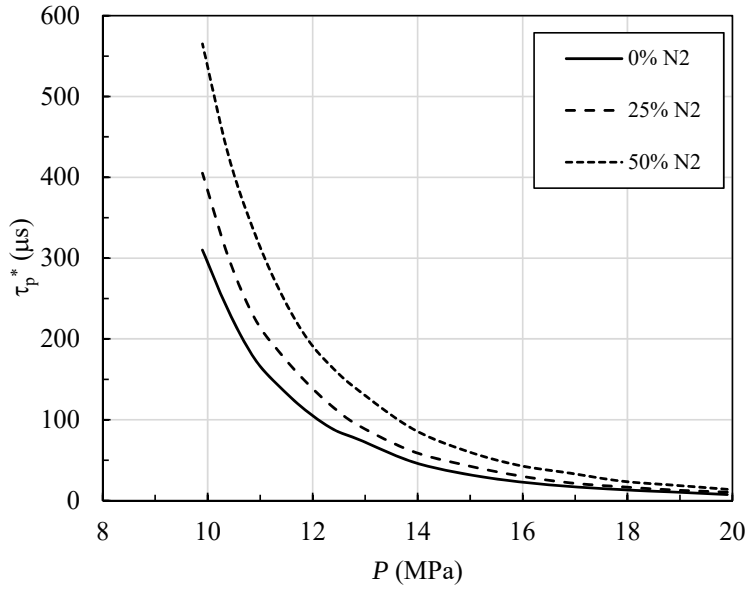

Figure 20: Critical volume pressure width parameter τ_P^* for a Gaussian pulse of pressure as a function of the peak pressure P_m for three nitrogen dilution levels in stoichiometric H_2-O_2 with the initial conditions of 101.325 kPa and 298.15 K.

8 Summary

Simplified models of the reaction of a gas volume under transient adiabatic compression conditions were developed and applied to the ignition of hydrogen-oxygen mixtures. These models were implemented using the Matlab and Cantera software environments to obtain numerical solutions for the thermodynamic state of the gas and species evolution with time. The chemical reaction mechanism used in this study was validated by comparisons with rapid compression ignition data.

The analytic critical decay rate model previously applied to shock ignition was validated for the case of exponential volume increase following instantaneous isentropic compression of stoichiometric mixtures initially at room temperature and pressure. For low-temperature (900-1050 K) and high-pressure (10-20 MPa) conditions following compression, analysis of the reaction pathways demonstrates that the rate limiting steps in the reaction zone involve the degenerate or straight chain processes dominated by the species H_2O_2 and HO_2.

A Gaussian pulse model of a volume transient was developed to examine the ignition under conditions of rapid compression immediately followed by decompression. Numerical simulations were used to determine critical pulse widths for explosion. For compression pulse durations (widths) less than the critical value, chemical reaction is quenched in the decompression phase and no explosion is observed. For stoichiometric hydrogen-oxygen mixtures, the computed critical pulse width parameter τ_v^* is found to be comparable to the critical decay time τ_e^* computed for the exponential volume increase model with the same peak compression ratio.

The effect of initial temperature, pressure and steam concentration was examined in a set of parametric computations. Initial temperature has the strongest impact on the critical decay time and critical pulse width. The effect of nitrogen addition is to increase the time scales but is much less effective than steam addition in this regard.

Acknowledgment

This work was partially supported by the U.S. Nuclear Regulatory Commission under Contract NRC-HQ-60-16-T-001, Caltech Task 1. Dr. Stephanie Coronel and Dr. Jean-Christophe Veilleux contributed to the development of the Gaussian pulse model and mechanism validation. Dr. Yunliang Qi carried out validation studies and computed the results shown in Figs. 16 and 17. Prof. Rémy Mével's review of the draft was extremely helpful in correcting and clarifying my exposition, he pointed out the importance of the work of Lamoureux et al. (2003) and motivated the reexamination of the issue of energetics.

A Adiabatic Explosion Parameters

Symbol	Eq.	Explanation
CR	(22)	compression ratio
T		temperature of compressed gas
P		pressure of compressed gas
t_i^*	(24)	constant volume time to explosion
t_r^*	(25)	constant volume energy release time
θ	(53)	nondimensional activation energy
$\gamma - 1$	(75)	effective ratio of specific heat minus one
n	(30)	effective reaction order
τ_e^*	(44)	critical value of expansion time
τ_v^*	(81)	critical value of pulse time

Table 1: Adiabatic explosion parameters for three models of ignition in compressed H_2 + $\frac{1}{2}O_2$ mixtures initially at 298.15 K and 101.325 kPa.

CR	T (K)	P (MPa)	t_i^* (s)	t_r^* (s)	θ	$\gamma - 1$	n	τ_e^* (s)	τ_v^* (s)
15	843.7	4.30	5.32×10^{-2}	4.76×10^{-9}	27.2	0.363	0.764	5.48×10^{-1}	3.51×10^{-1}
16	863.7	4.70	2.80×10^{-2}	4.38×10^{-9}	26.5	0.362	0.768	2.76×10^{-1}	1.90×10^{-1}
17	882.8	5.10	1.56×10^{-2}	4.05×10^{-9}	25.9	0.361	0.770	1.50×10^{-1}	1.08×10^{-1}
18	901.2	5.51	9.14×10^{-3}	3.77×10^{-9}	25.3	0.360	0.773	8.54×10^{-2}	6.47×10^{-2}
19	918.9	5.93	5.57×10^{-3}	3.52×10^{-9}	24.7	0.359	0.774	5.12×10^{-2}	4.08×10^{-2}
20	935.9	6.36	3.53×10^{-3}	3.30×10^{-9}	24.2	0.358	0.776	3.14×10^{-2}	2.57×10^{-2}
21	952.3	6.80	2.30×10^{-3}	3.11×10^{-9}	23.8	0.357	0.776	2.06×10^{-2}	1.68×10^{-2}
22	968.3	7.24	1.54×10^{-3}	2.94×10^{-9}	23.4	0.356	0.777	1.35×10^{-2}	1.17×10^{-2}
23	983.7	7.69	1.06×10^{-3}	2.78×10^{-9}	23.0	0.355	0.777	9.01×10^{-3}	8.18×10^{-3}
24	998.7	8.15	7.47×10^{-4}	2.63×10^{-9}	22.6	0.355	0.777	6.26×10^{-3}	5.71×10^{-3}
25	1013.0	8.61	5.36×10^{-4}	2.50×10^{-9}	22.3	0.354	0.777	4.44×10^{-3}	4.20×10^{-3}
26	1027.0	9.08	3.92×10^{-4}	2.40×10^{-9}	22.0	0.353	0.777	3.17×10^{-3}	3.09×10^{-3}
27	1041.0	9.55	2.91×10^{-4}	2.28×10^{-9}	21.7	0.352	0.776	2.39×10^{-3}	2.39×10^{-3}
28	1055.0	10.04	2.20×10^{-4}	2.18×10^{-9}	21.5	0.352	0.775	1.73×10^{-3}	1.76×10^{-3}
29	1068.0	10.52	1.68×10^{-4}	2.09×10^{-9}	21.2	0.351	0.774	1.30×10^{-3}	1.36×10^{-3}
30	1080.0	11.02	1.30×10^{-4}	2.01×10^{-9}	21.0	0.350	0.773	9.96×10^{-4}	1.11×10^{-3}
31	1093.0	11.51	1.02×10^{-4}	1.92×10^{-9}	20.8	0.349	0.772	7.76×10^{-4}	8.56×10^{-4}
32	1105.0	12.02	8.06×10^{-5}	1.86×10^{-9}	20.5	0.349	0.771	6.01×10^{-4}	6.97×10^{-4}
33	1117.0	12.53	6.45×10^{-5}	1.80×10^{-9}	20.3	0.348	0.770	4.72×10^{-4}	5.68×10^{-4}
34	1129.0	13.04	5.20×10^{-5}	1.72×10^{-9}	20.2	0.347	0.768	3.78×10^{-4}	4.62×10^{-4}
35	1140.0	13.56	4.23×10^{-5}	1.66×10^{-9}	20.0	0.347	0.767	3.02×10^{-4}	3.77×10^{-4}
36	1151.0	14.08	3.47×10^{-5}	1.61×10^{-9}	19.8	0.346	0.765	2.51×10^{-4}	3.07×10^{-4}
37	1162.0	14.61	2.87×10^{-5}	1.56×10^{-9}	19.7	0.345	0.764	2.01×10^{-4}	2.63×10^{-4}
38	1173.0	15.15	2.39×10^{-5}	1.51×10^{-9}	19.5	0.345	0.762	1.65×10^{-4}	2.14×10^{-4}
39	1183.0	15.69	2.00×10^{-5}	1.47×10^{-9}	19.3	0.344	0.761	1.38×10^{-4}	1.84×10^{-4}
40	1194.0	16.23	1.69×10^{-5}	1.41×10^{-9}	19.2	0.343	0.759	1.15×10^{-4}	1.58×10^{-4}
41	1204.0	16.78	1.43×10^{-5}	1.38×10^{-9}	19.1	0.343	0.757	9.71×10^{-5}	1.36×10^{-4}
42	1214.0	17.33	1.22×10^{-5}	1.34×10^{-9}	18.9	0.342	0.755	8.09×10^{-5}	1.16×10^{-4}
43	1224.0	17.88	1.04×10^{-5}	1.30×10^{-9}	18.8	0.342	0.754	6.89×10^{-5}	9.96×10^{-5}
44	1233.0	18.44	8.97×10^{-6}	1.27×10^{-9}	18.7	0.341	0.752	5.86×10^{-5}	8.54×10^{-5}
45	1243.0	19.01	7.75×10^{-6}	1.23×10^{-9}	18.6	0.341	0.750	4.98×10^{-5}	7.32×10^{-5}
46	1252.0	19.58	6.73×10^{-6}	1.20×10^{-9}	18.5	0.340	0.748	4.33×10^{-5}	6.61×10^{-5}

CR	T (K)	P (MPa)	t_i^* (s)	t_r^* (s)	θ	$\gamma - 1$	n	τ_e^* (s)	τ_v^* (s)
47	1261.0	20.15	5.87×10^{-6}	1.18×10^{-9}	18.4	0.340	0.746	3.76×10^{-5}	5.66×10^{-5}
48	1270.0	20.72	5.13×10^{-6}	1.14×10^{-9}	18.3	0.339	0.745	3.24×10^{-5}	5.11×10^{-5}
49	1279.0	21.30	4.51×10^{-6}	1.11×10^{-9}	18.2	0.339	0.743	2.81×10^{-5}	4.38×10^{-5}
50	1288.0	21.89	3.97×10^{-6}	1.09×10^{-9}	18.1	0.338	0.741	2.49×10^{-5}	3.96×10^{-5}

B Comparison of Three Diluents

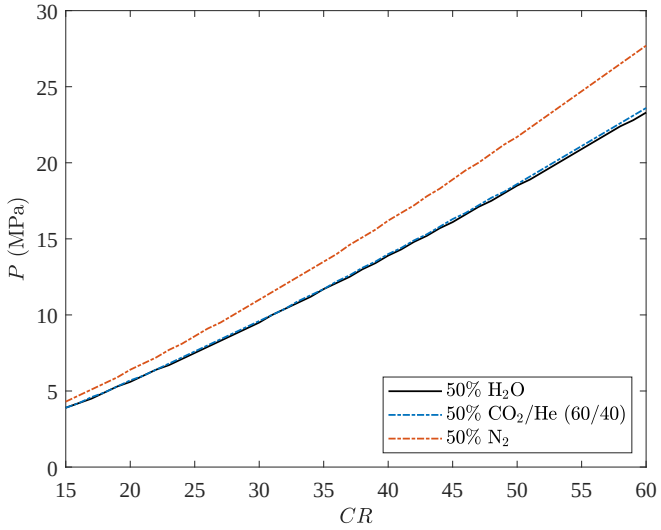

Figure 21: Peak pressure as a function of the compression ratio CR for three dilution gases in stoichiometric H_2-O_2 mixtures with the initial conditions of 101.325 kPa and 298.15 K. Calculations performed using the Keromnes et al. (2013) reaction mechanism.

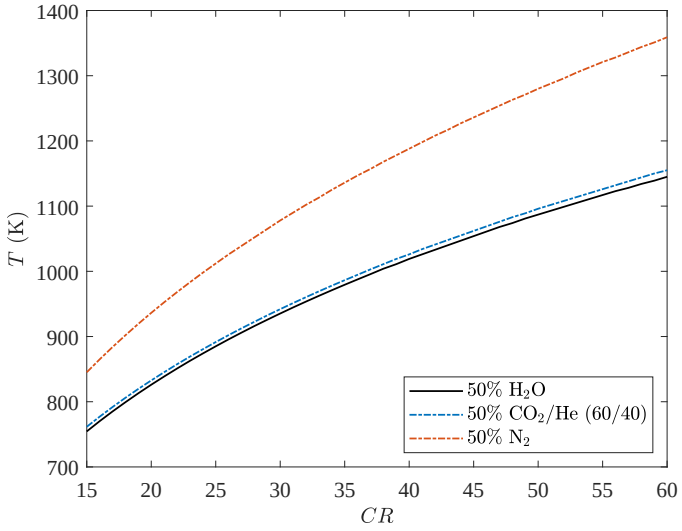

Figure 22: Peak temperature as a function of the compression ratio CR for three dilution gases in stoichiometric H_2-O_2 mixtures with the initial conditions of 101.325 kPa and 298.15 K. Calculations performed using the Keromnes et al. (2013) reaction mechanism.

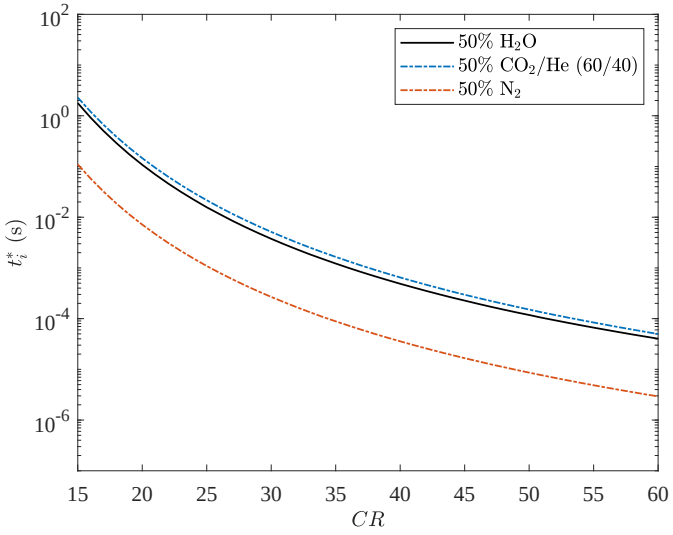

Figure 23: Induction time as a function of the compression ratio CR for three dilution gases in stoichiometric H_2-O_2 mixtures with the initial conditions of 101.325 kPa and 298.15 K. Calculations performed using the Keromnes et al. (2013) reaction mechanism.

C Analysis of Energy Equation

The energy equation (7) for the constant volume (v = constant) case can be written as the sum of contributions from the reactions of each species

$$\frac{\mathrm{d}T}{\mathrm{d}t} = \underbrace{-\frac{e_1}{cv}\frac{\mathrm{d}Y_1}{\mathrm{d}t}}_{\dot{T}_{k=1}} + \underbrace{-\frac{e_2}{cv}\frac{\mathrm{d}Y_2}{\mathrm{d}t}}_{\dot{T}_{k=2}} + \ldots + \underbrace{-\frac{e_K}{cv}\frac{\mathrm{d}Y_K}{\mathrm{d}t}}_{\dot{T}_{k=K}} . \tag{102}$$

The net contribution of each species k to the conversion of chemical to thermal energy can be expressed as a fraction F_k of the total adiabatic temperature rise ΔT_a contributed by the reaction of that species

$$F_k = \frac{\Delta T_k}{\Delta T_a} , \tag{103}$$

where

$$\Delta T_k = \int_0^\infty \dot{T}_k \, \mathrm{d}t , \tag{104}$$

$$= \int_0^\infty -\frac{e_k}{cv}\frac{\mathrm{d}Y_k}{\mathrm{d}t} \, \mathrm{d}t . \tag{105}$$

The integral can be evaluated once the full solution is computed for $T(t)$ and $Y_k(t)$. Using the same conditions as in Fig. 1, this analysis was carried out and the results are shown in Fig. 24 and 25. The fraction contributions to the total temperature increase (103) are given in Table 2.

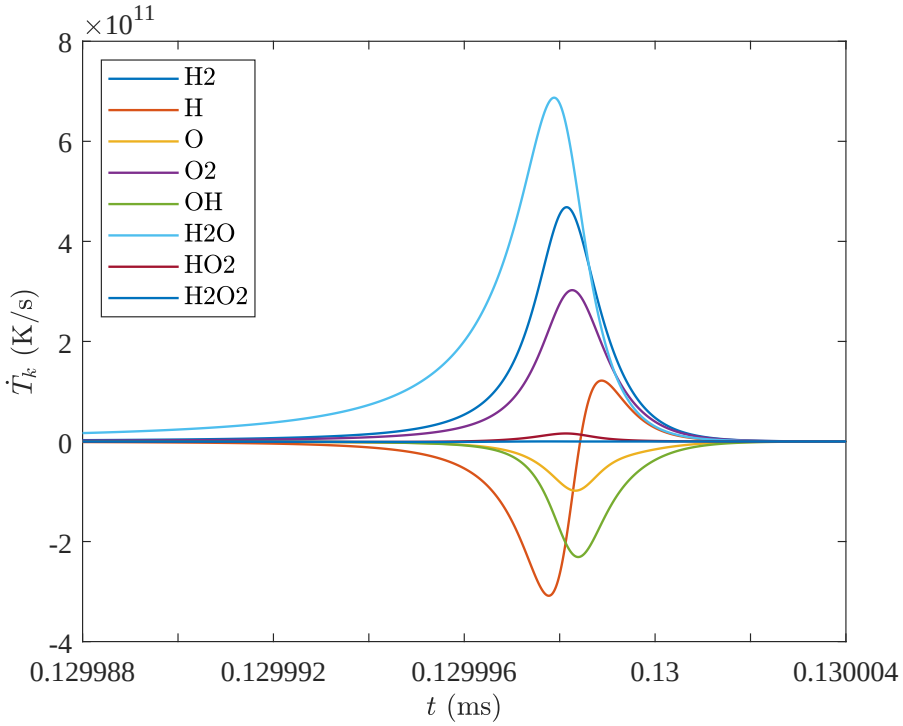

Figure 24: Individual species contributions to temperature rate of change. Analysis of constant volume combustion for a stoichiometric H_2-O_2 mixture with the conditions used in Fig. 1.

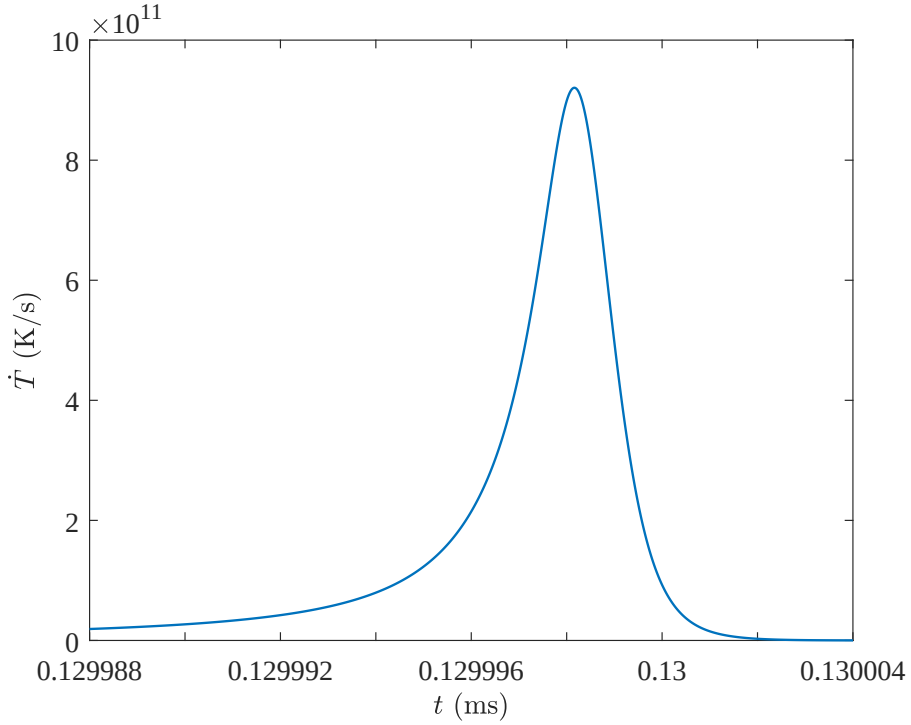

Figure 25: Temperature rate of change due to all species. Analysis of constant volume combustion for a stoichiometric H_2-O_2 mixture with the conditions used in Fig. 1.

Table 2: Fractional contribution of each species to the total temperature rise for the conditions of Fig. 1.

H_2	0.33043
H	-0.11158
O	-0.059776
O_2	0.21491
OH	-0.12941
H_2O	0.74873
HO_2	0.0038188
H_2O_2	0.0028949

To further delve into the contributions to the energy equation, the contributions by specific reactions are examined. The reaction rate for each species can be written in terms of the net rate of progress $\dot{q}_j$ for each reaction j and the net stoichiometric coefficients ν_{kj} for the production (or destruction) of species k in reaction j. The net molar product rate of species k in a reaction network with J reactions is

$$\dot{\omega}_k = \sum_{j=1}^{J} \nu_{kj} \dot{q}_j \ . \tag{106}$$

The energy equation for constant-volume reaction can be written in terms of the rate of progress variables as

$$\frac{\mathrm{d}T}{\mathrm{d}t} = -\frac{1}{\rho c_v} \sum_{k=1}^{K} e_k W_k \sum_{j=1}^{J} \nu_{kj} \dot{q}_j \ . \tag{107}$$

Interchanging the order of summation, we have

$$\frac{\mathrm{d}T}{\mathrm{d}t} = \sum_{j=1}^{J} \left(-\frac{1}{\rho c_v} \sum_{k=1}^{K} e_k W_k \nu_{kj} \right) \dot{q}_j \ , \tag{108}$$

which can be written as a sum of contributions from each reaction

$$= \underbrace{\left(-\frac{1}{\rho c_v} \sum_{k=1}^{K} e_k W_k \nu_{k1} \right) \dot{q}_1}_{\dot{T}_{j=1}} + \underbrace{\left(-\frac{1}{\rho c_v} \sum_{k=1}^{K} e_k W_k \nu_{k2} \right) \dot{q}_2}_{\dot{T}_{j=2}} \quad + \quad \ldots \quad + \quad \underbrace{\left(-\frac{1}{\rho c_v} \sum_{k=1}^{K} e_k W_k \nu_{kJ} \right) \dot{q}_J}_{\dot{T}_{j=J}} \ . \tag{109}$$

There are a subset of reactions that contribute the majority of the total conversion of chemical to thermal energy for the case of Fig. 1. These reactions, percentage of total contribution, and the enthalpy of reaction at the initial state are given in Table 3. The fractional contribution of each reaction to the total temperature rise is

$$F_j = \frac{\Delta T_j}{\Delta T_a} \ , \tag{110}$$

$$\Delta T_j = \int_0^\infty \dot{T}_j \, \mathrm{d}t \ , \tag{111}$$

$$= \int_0^\infty \left(-\frac{1}{\rho c_v} \sum_{k=1}^{K} e_k W_k \nu_{kj} \right) \dot{q}_j \, \mathrm{d}t \ . \tag{112}$$

Table 3: Fractional total temperature rise due to the reactions dominating the contribution to the total temperature rise for the conditions of Fig. 1. Reaction numbers are as given in the Hong et al. (2011) reaction mechanism (these are not the same as used in the main text), heat of reaction $\Delta_r H$ is given in MJ·kmol^{-1}.

R_H#	Reaction	F_j	$\Delta_r H$
17	$H_2 + OH \rightleftarrows H + H_2O$	0.260	-52.4
5	$H + O_2 (+H_2O) \rightleftarrows HO_2 (+H_2O)$	0.185	-220.
2	$H + O_2 (+M) \rightleftarrows HO_2 (+M)$	0.184	-220.
13	$H_2O + H_2O \rightleftarrows H + H_2O + OH$	0.175	+516.
20	$H + HO_2 \rightleftarrows H_2 + O_2$	0.102	-243.
18	$H + HO_2 \rightleftarrows OH + OH$	0.088	-179
6	$H_2O_2 (+M) \rightleftarrows OH + OH \ (+M)$	-0.097	+202.
1	$H + O_2 \rightleftarrows O + OH$	-0.127	+57.8

The contributions of each of the reactions in Table 3 are shown for the time frame of significant energy release in Figures 26 to 33. Reactions R_H17, R_H5, R_H2, R_H13, R_H20, R_H18 all contribute positively throughout the reaction process to the chemical-to-thermal energy conversion. All of those reactions except R_H13 have a negative enthalpy of reaction $\Delta_r H$ indicating that these reactions progress in the forward direction (from left to right as written in Table 3) throughout the reaction process, while R_H13 has a positive heat of reaction and progresses in the reverse direction (from right to left as written in Table 3). Two reactions, R_H6 and R_H1, contributed negatively to the chemical-to-thermal energy conversion throughout the reaction process. These reactions have positive heats of reaction so these progress in the forward direction (from left to right as written in Table 3) throughout the reaction process.

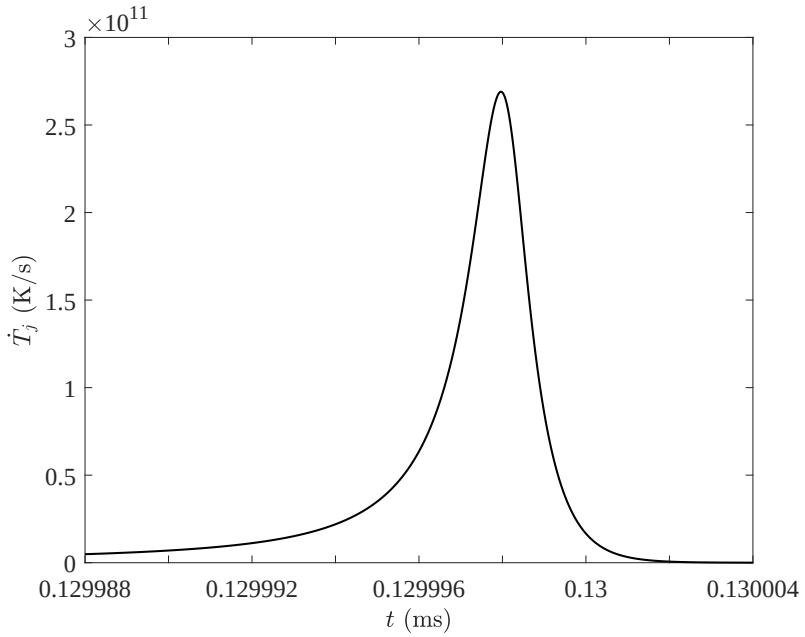

Figure 26: Reaction R_H17 (H_2 + OH $\rightleftarrows$ H + H_2O) contributions to temperature rate of change. Analysis of constant volume combustion for a stoichiometric H_2-O_2 mixture with the conditions used in Fig. 1.

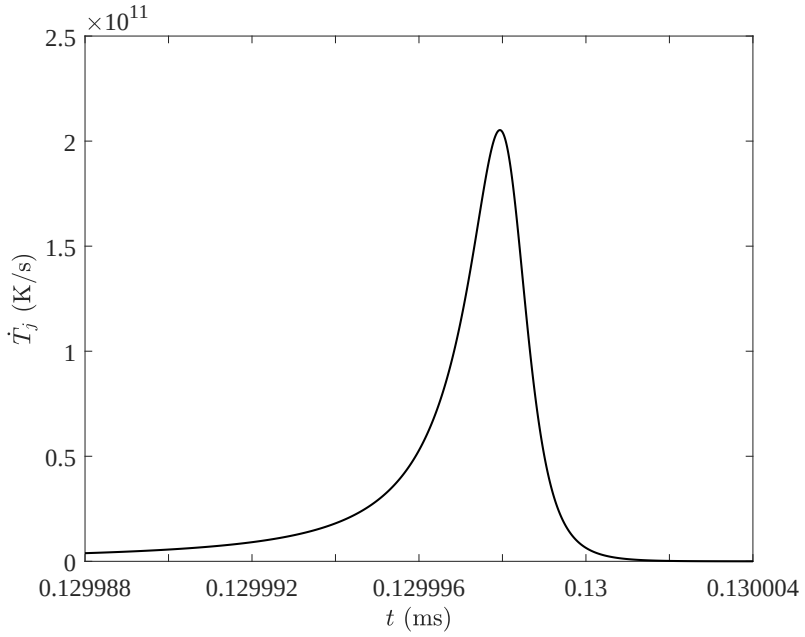

Figure 27: Reaction R_H5 (H + O_2 (+H_2O) $\rightleftarrows$ HO_2 (+H_2O)) contributions to temperature rate of change. Analysis of constant volume combustion for a stoichiometric H_2-O_2 mixture with the conditions used in Fig. 1.

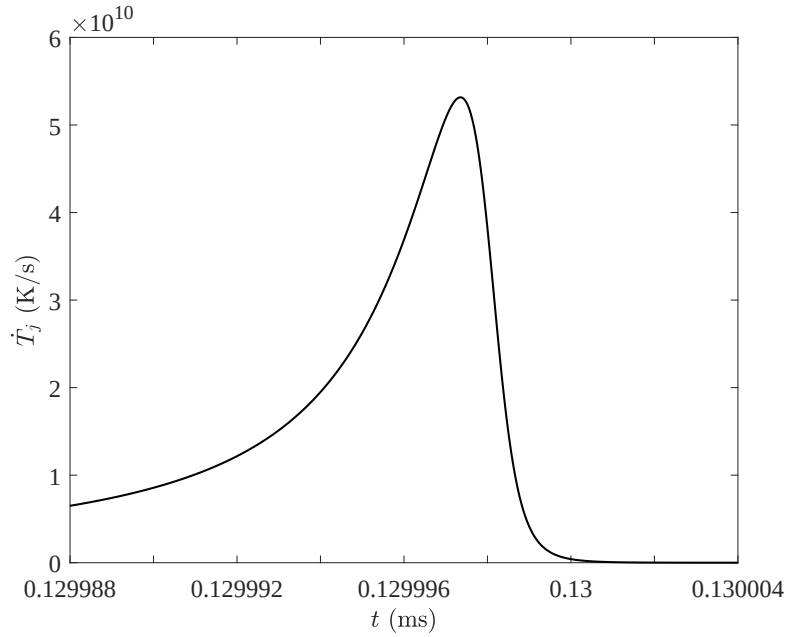

Figure 28: Reaction R_H2 (H + O_2 (+M) $\rightleftarrows$ HO_2 (+M)) contributions to temperature rate of change. Analysis of constant volume combustion for a stoichiometric H_2-O_2 mixture with the conditions used in Fig. 1.

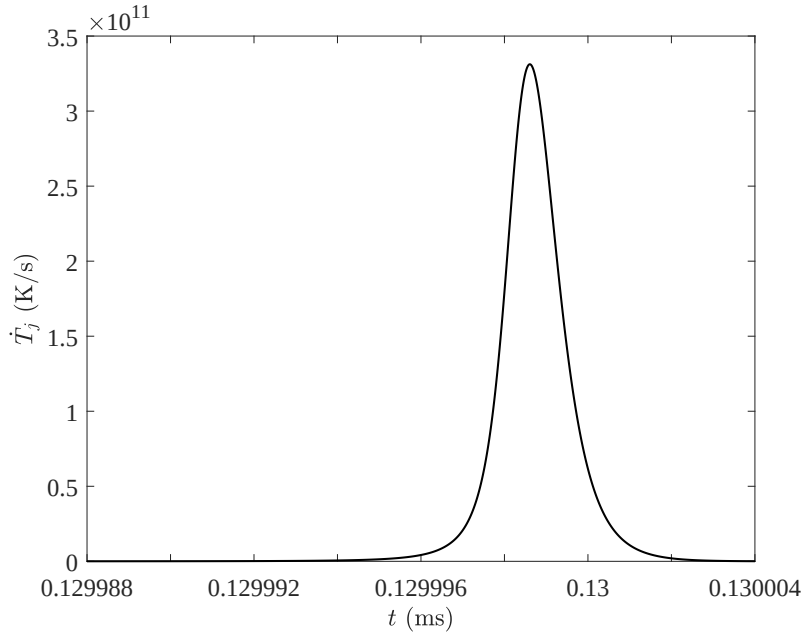

Figure 29: Reaction R_H13 (H_2O + H_2O $\rightleftarrows$ H + H_2O + OH) contributions to temperature rate of change. Analysis of constant volume combustion for a stoichiometric H_2-O_2 mixture with the conditions used in Fig. 1.

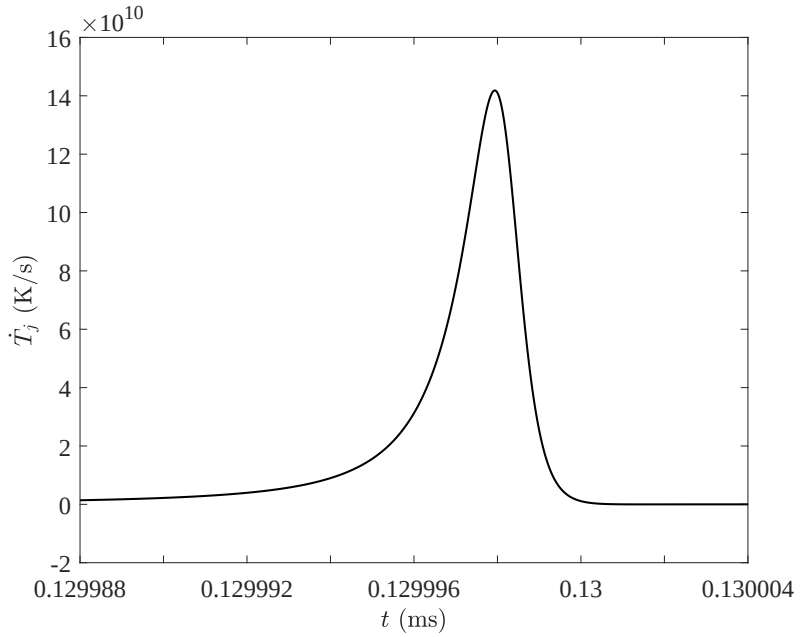

Figure 30: Reaction R_H20 ($H + HO_2 \rightleftarrows H_2 + O_2$) contributions to temperature rate of change. Analysis of constant volume combustion for a stoichiometric H_2-O_2 mixture with the conditions used in Fig. 1.

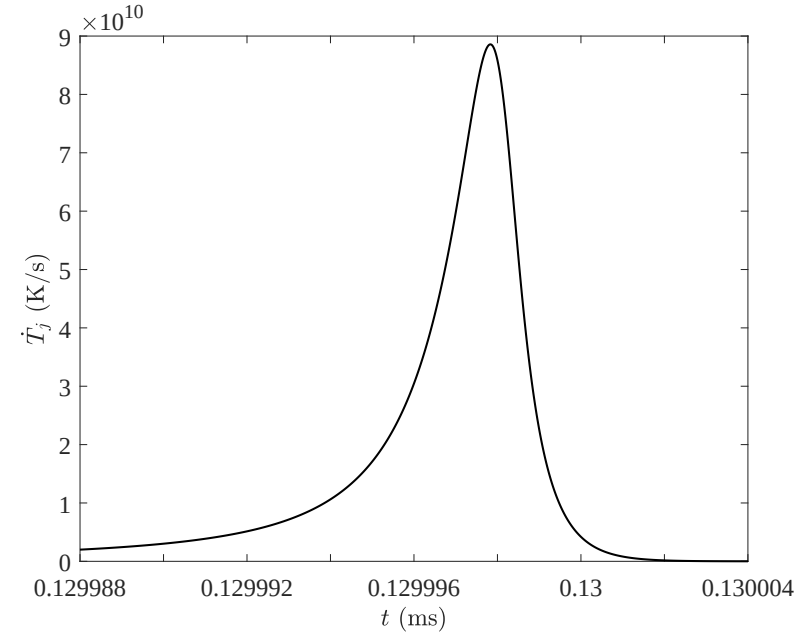

Figure 31: Reaction R_H18 ($H + HO_2 \rightleftarrows OH + OH$) contributions to temperature rate of change. Analysis of constant volume combustion for a stoichiometric H_2-O_2 mixture with the conditions used in Fig. 1.

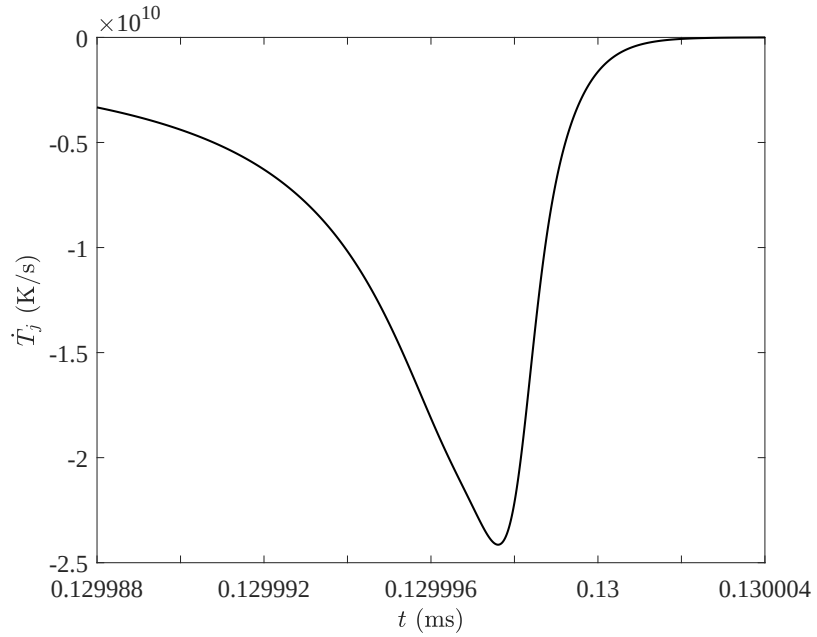

Figure 32: Reaction R_H6 (H_2O_2 (+M) $\rightleftarrows$ OH + OH (+M)) contributions to temperature rate of change. Analysis of constant volume combustion for a stoichiometric H_2-O_2 mixture with the conditions used in Fig. 1.

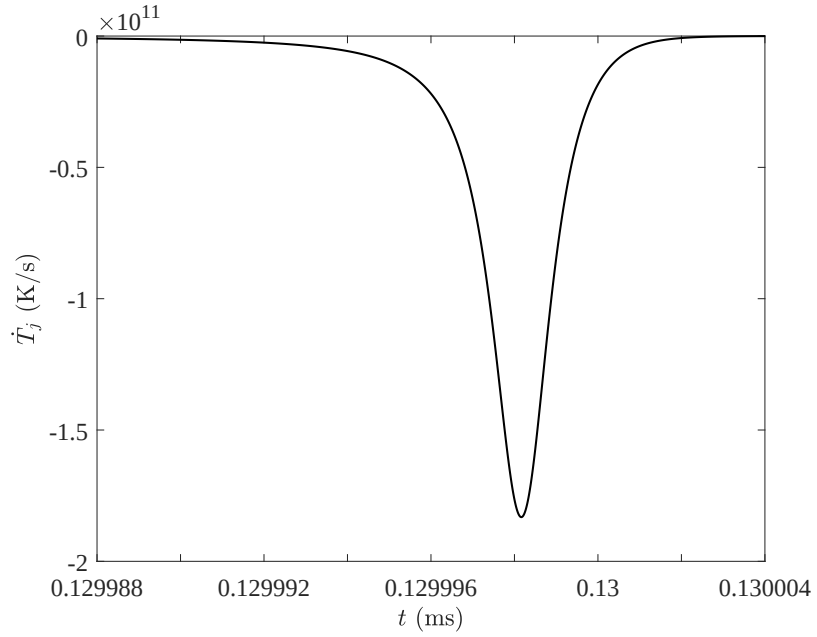

Figure 33: Reaction R_H1 (H + O_2 $\rightleftarrows$ O + OH) contributions to temperature rate of change. Analysis of constant volume combustion for a stoichiometric H_2-O_2 mixture with the conditions used in Fig. 1.

References

S. P. M. Bane, J. L. Zeigler, and J.E. Shepherd. Development of One-Step Chemistry Models for Flame and Ignition Simulation. Technical Report GALCIT Report FM2010.002, California Institute of Technology, Pasadena, CA 91125, 2010. 6

F. Battin-Leclerc. Detailed chemical kinetic models for the low-temperature combustion of hydrocarbons with application to gasoline and diesel fuel surrogates. *Progress in Energy and Combustion Science*, 34(4):440–498, August 2008. 11

L.R. Boeck, R. Mével, and T. Sattelmayer. Models for shock-induced ignition evaluated by detailed chemical kinetics for hydrogen/air in the context of deflagration-to-detonation transition. *Journal of Loss Prevention in the Process Industries*, 49:731–738, September 2017. 12

P.A. Boettcher, R. Mével, V. Thomas, and J.E. Shepherd. The effect of heating rates on low temperature hexane air combustion. *Fuel*, 96:392–403, 2012. 4

P.A. Boettcher, V. Thomas, and R. Mével. Thermal ignition - one-step modeling of the transition from slow reactions to ignition. In *Proceedings of the Western States Section Meeting of the Combustion Institute, , March 24 2014.*, Pasadena, USA, 2014. 4

Richard S. Brokaw. Analytic solutions to the ignition kinetics of the hydrogen-oxygen reaction. *Symposium (International) on Combustion*, 10(1):269–278, January 1965. 12

S. Browne, Z. Liang, and J. E. Shepherd. Detailed and Simplified Chemical Reaction Mechanisms for Detonation Simulation. In *Fall 2005 Western States Section of the Combustion Institute, Paper 05F-21*, Stanford, CA, Oct. 17-18, 2005. 12

J. D. Buckmaster and G. S. S. Ludford. *Theory of Laminar Flames*. Cambridge University Press, 1982. 15

Terrence M Cain. *Compression Ignition Driven Shock Tubes*. MS, University of Queensland, Brisbane, Australia, July 1986. 13, 14

T.M. Cain. Autoignition of hydrogen at high pressure. *Combustion and Flame*, 111(1-2):124–132, October 1997. 14

M. F. Campbell, T. Parise, A. M. Tulgestke, R. M. Spearrin, D. F. Davidson, and R. K. Hanson. Strategies for obtaining long constant-pressure test times in shock tubes. *Shock Waves*, 25(6):651–665, November 2015a. 3

Matthew F. Campbell, Shengkai Wang, Christopher S. Goldenstein, R. Mitchell Spearrin, Andrew M. Tulgestke, Luke T. Zaczek, David F. Davidson, and Ronald K. Hanson. Constrained reaction volume shock tube study of n -heptane oxidation: Ignition delay times and time-histories of multiple species and temperature. *Proceedings of the Combustion Institute*, 35(1):231–239, 2015b. 3

Matthew F. Campbell, Kyle G. Owen, David F. Davidson, and Ronald K. Hanson. Dependence of Calculated Postshock Thermodynamic Variables on Vibrational Equilibrium and Input Uncertainty. *Journal of Thermophysics and Heat Transfer*, 31(3):586–608, July 2017. 3

Marcos Chaos and Frederick L. Dryer. Chemical-kinetic modeling of ignition delay: Considerations in interpreting shock tube data. *Int. J. Chem. Kinet.*, 42(3):143–150, March 2010. 3

S.A. Coronel, J.-C. Veilleux, and J. E. Shepherd. Ignition of Stoichiometric Hydrogen-Oxygen by Water Hammer. *Proceedings of the Combustion Institute*, 38, 2020. 1, 23, 27, 28, 29

Apurba K. Das, Chih-Jen Sung, Yu Zhang, and Gaurav Mittal. Ignition delay study of moist hydrogen/oxidizer mixtures using a rapid compression machine. *International Journal of Hydrogen Energy*, 37(8):6901–6911, April 2012. 13, 21, 22

C. A. Eckett, J. J. Quirk, and and J. E. Shepherd. The role of unsteadiness in direct initiation of gaseous detonations. *Journal of Fluid Mechanics*, 421:147–183, 2000. 15, 20

D. Fernández-Galisteo, A.L. Sánchez, A. Liñán, and F.A. Williams. One-step reduced kinetics for lean hydrogen–air deflagration. *Combustion and Flame*, 156(5):985–996, May 2009. 13

D.A. Frank-Kamenetskii. *Diffusion and Heat Exchange in Chemical Kinetics*. Princeton University Press, 1955. 18

S. Scott Goldsborough, Colin Banyon, and Gaurav Mittal. A computationally efficient, physics-based model for simulating heat loss during compression and the delay period in RCM experiments. *Combustion and Flame*, 159 (12):3476–3492, December 2012. 3

S.S. Goldsborough, S. Hochgreb, G. VanHove, M. Woolridge, H.J. Curran, and C-J. Sung. Advances in rapid compression machine studies of low- and intermediate-temperature autoignition phenomena. *Prog. Energy Combust. Sci.*, 63:1–78, 2017. 2, 21

David G. Goodwin, Harry K. Moffat, and Raymond L. Speth. Cantera: An Object-oriented Software Toolkit for Chemical Kinetics, Thermodynamics, and Transport Processes, 2017. 5

K. P. Grogan and M. Ihme. Identification of governing physical processes of irregular combustion through machine learning. *Shock Waves*, 28(5):941–954, September 2018. 3

Kevin Grogan, Qing Wang, and Matthias Ihme. Modeling Gas Dynamic Effects in Shock-Tubes for Reaction Kinetics Measurements. In *53rd AIAA Aerospace Sciences Meeting*, Kissimmee, Florida, January 2015. American Institute of Aeronautics and Astronautics. 3

Hamid Hashemi, Jakob M. Christensen, Sander Gersen, and Peter Glarborg. Hydrogen oxidation at high pressure and intermediate temperatures: Experiments and kinetic modeling. *Proceedings of the Combustion Institute*, 35(1): 553–560, 2015. 14

Zekai Hong, David F. Davidson, and Ronald K. Hanson. An improved H-2/O-2 mechanism based on recent shock tube/laser absorption measurements. *Combustion and Flame*, 158(4, SI):633–644, April 2011. 5, 6, 7, 13, 15, 21, 24, 27, 39

A. K. Kapila. *Asymptotic Treatment of Chemically Reacting Systems*. Pitman Publishing Inc, 1983. 15

Alan Keromnes, Wayne K. Metcalfe, Karl A. Heufer, Nicola Donohoe, Apurba K. Das, Chih-Jen Sung, Juergen Herzler, Clemens Naumann, Peter Griebel, Olivier Mathieu, Michael C. Krejci, Eric L. Petersen, William J. Pitz, and Henry J. Curran. An experimental and detailed chemical kinetic modeling study of hydrogen and syngas mixture oxidation at elevated pressures. *Combustion and Flame*, 160(6):995–1011, June 2013. 35, 36

Alexander A. Konnov. Yet another kinetic mechanism for hydrogen combustion. *Combustion and Flame*, 203:14–22, May 2019. 14

W Kordylewski and S.K. Scott. The Influence of Self-Heating on the Second and Third Explosion Limits in the 02 + H2 Reaction. *Combust. Flame*, 57:127–139, 1984. 13

N Lamoureux, N Djebaïli-Chaumeix, and C.-E Paillard. Laminar flame velocity determination for H2–air–He–CO2 mixtures using the spherical bomb method. *Experimental Thermal and Fluid Science*, 27(4):385–393, April 2003. 28, 32

D Lee and S Hochgreb. Hydrogen autoignition at pressures above the second explosion limit (0.6-4.0 MPa). *International Journal of Chemical Kinetics*, 30(6):385–406, June 1998. 13, 14

B. Lewis and G. von Elbe. *Combustion, Flames and Explosions of Gases*. Academic Press, New York, NY USA, second edition, 1961. 12

H. Li, Z. C. Owens, D. F. Davidson, and R. K. Hanson. A simple reactive gasdynamic model for the computation of gas temperature and species concentrations behind reflected shock waves. *Int. J. Chem. Kinet.*, 40(4):189–198, April 2008. 3

Wenkai Liang and Chung K. Law. An analysis of the explosion limits of hydrogen/oxygen mixtures with nonlinear chain reactions. *Phys. Chem. Chem. Phys.*, 20(2):742–751, 2018. 13

Z. Liang, S. Browne, R. Deiterding, and J. E. Shepherd. Detonation Front Structure and the Competition for Radicals. In *Proceedings of the 31rst Combustion Institute*, volume 31, pages 2445–2453, 2007. 13

U. Maas and J. Warnatz. Ignition processes in hydrogen-oxygen mixtures. *Combustion and Flame*, 74(1):53–69, October 1988. 13

B.M. Maxwell and M.I. Radulescu. Ignition limits of rapidly expanding diffusion layers: Application to unsteady hydrogen jets. *Combustion and Flame*, 158(10):1946–1959, October 2011. 15

J. Melguizo-Gavilanes, P.A. Boettcher, R. Mével, and J.E. Shepherd. Numerical study of the transition between slow reaction and ignition in a cylindrical vessel. *Combustion and Flame*, 204:116–136, June 2019. 4

R. Mével, J. Melguizo-Gavilanes, and D. Davidenko. Ignition of hydrogen-air mixtures under volumetric expansion. *Proceedings of the Combustion Institute*, 37(3):3503–3511, 2019. 15

David W. Mikolaitis. An Asymptotic Analysis of the Induction Phases of Hydrogen-Air Detonations. *Combustion Science and Technology*, 52(4-6):293–323, April 1987. 13

Carsten Olm, István Gy. Zsély, Róbert Pálvölgyi, Tamás Varga, Tibor Nagy, Henry J. Curran, and Tamás Turányi. Comparison of the performance of several recent hydrogen combustion mechanisms. *Combustion and Flame*, 161 (9):2219–2234, September 2014. 14

Matei I. Radulescu and Brian M. Maxwell. Critical ignition in rapidly expanding self-similar flows. *Physics of Fluids*, 22(6):066101, June 2010. 15

Dennis L. Ripley and W. C. Gardiner. Shock-Tube Study of the Hydrogen—Oxygen Reaction. II. Role of Exchange Initiation. *The Journal of Chemical Physics*, 44(6):2285–2296, March 1966. 12

Antonio L. Sánchez, Eduardo Fernández-Tarrazo, and Forman A. Williams. The chemistry involved in the third explosion limit of H2–O2 mixtures. *Combustion and Flame*, 161(1):111–117, January 2014. 13

G. L. Schott and J. L. Kinsey. Kinetic Studies of Hydroxyl Radicals in Shock Waves. II. Induction Times in the Hydrogen-Oxygen Reaction. *The Journal of Chemical Physics*, 29(5):1177–1182, November 1958. 12

N. N. Semenov. *Some Problems in Chemical Kinetics and Reactivity - Two Volumes*. Princeton University Press, Princeton New Jersey, 1959. 4, 11, 12, 18

J. Shepherd. Chemical Kinetics of Hydrogen-Air-Diluent Detonations. In *Dynamics of Explosions*, volume 106 of *Progress in Astronautics and Aeronautics*, pages 263–293. AIAA, 1986. 13

Gordon B. Skinner and Gordon H. Ringrose. Ignition Delays of a Hydrogen—Oxygen—Argon Mixture at Relatively Low Temperatures. *The Journal of Chemical Physics*, 42(6):2190–2192, March 1965. 12

Jean-Christophe Veilleux, Stephanie A. Coronel, and Joseph E. Shepherd. Ignition by Water Hammer. GALCIT EDL2019.001, California Institute of Technology, Pasadena, CA (USA), December 2019. 21, 23, 27, 28, 29